POLITECNICO DI MILANO

Facoltà di Ingegneria Industriale

Corso di Laurea in
Ingegneria Spaziale

COUPLING OF LUMPED AND DISTRIBUTED PARAMETER MODELS FOR NUMERICAL SIMULATION OF A SINTERED HEAT PIPE

Relatore: Prof. Luigi VIGEVANO

Co-relatore: Prof. Marco MARENGO

Tesi di Laurea di:

Filomena IORIZZO Matr. 712311

Anno Accademico 2010 - 2011

COUPLING OF LUMPED AND DISTRIBUTED PARAMETER MODELS FOR NUMERICAL SIMULATION OF A SINTERED HEAT PIPE

To my family

Acknowledgments

First of all I would like to express my deepest gratitude to my thesis supervisors:
Prof. Luigi Vigevano for his professionalism, kindness and for his valuable suggestions,
Prof. Marco Marengo for his guidance, support and motivation and for his thoughtful discussions that will be a source of inspiration in my future engineering career.
I should express my appreciation to
Prof . Alfonso Niro who piqued my interest in thermal analysis,
Prof. Luca Formaggia for the priceless suggestions that helped me to address numerical issues.
I am deeply indebted to Mauro Mameli for his invaluable help in writing this thesis and for all his support. Thanks Mauro!
I must thank the *crew* of Thermal Physics Laboratory for the enjoyable time spent together.
Special thanks should also go to my family: my mum and my aunt Luisa for their endless love and support, my father and my brother who always believe in me.
Thinking about the last years of my university career at "Politecnico di Milano", I am very grateful to my charming friend Nicola, whose determination inspired me, and to all my friends, especially Chiara, Simone and Roberto, for their affection.
Thank you Stefano for your love and patience and for the pleasant time we have together.

Now I am free:…

I believe it. You can do it too.

Contents

Sommario

Un heat pipe è un dispositivo di scambio termico costituito da un tubo sigillato in grado di trasportare una grande quantità di potenza termica sfruttando il passaggio di fase di un fluido posto al suo interno e le forze capillari sviluppate da una struttura porosa collocata sulla parete interna.
Le prestazioni dell'heat pipe sono in genere stimate tramite modelli a parametri concentrati, i quali però non sono in grado di rappresentare accuratamente l'interazione tra l'heat pipe e il componente solido da raffreddare. È stato quindi sviluppato un programma per una simulazione ibrida basata sull'integrazione di un modello a parametri concentrati in un solutore a volumi finiti in modo da eseguire un'analisi termica accoppiata (ibrida). I due modelli sono legati dalle condizioni al contorno sulla superficie d'interfaccia.
Dopo un breve cenno ai principi di funzionamento, ai limiti e vantaggi di un heat pipe si procede all'introduzione del modello a parametri concentrati non stazionario, spiegando come è stato accoppiato numericamente ad un solutore a volumi finiti. Infine i risultati delle analisi sono confrontati con quelli ottenuti da un modello a elementi finiti in cui l'heat pipe è modellato come un mezzo con alta conducibilità termica.
L'obiettivo di questa tesi è fornire un solutore ibrido utile per un'efficiente progettazione di un heat pipe, puntando ad una sua ampia diffusione grazie all'uso di programmi open source come OpenFOAM.

Parole chiave: heat pipe, analisi non stazionaria, modello a parametri concentrati, modello a volumi finiti, analisi ibrida, OpenFOAM

Abstract

Heat pipes are capillary driven two-phase heat transfer devices based on the evaporation/condensation of a working fluid. Their major advantages with respect to traditional heat transfer devices are the ability to operate against gravity and to have a greater maximum heat transport capability. A literature review is carried out in order to describe heat pipe operation and design, transfer limitations, and how various parameters affect the heat pipe's operational characteristics.
The heat pipe performances are generally investigated by lumped parameter analyses, however the interaction with heat source solid components can not be properly accounted for. For this purpose a hybrid solver, based on the integration of a heat pipe lumped parameter model with a finite volume model of the external solid where the heat pipe is embedded, is developed in order to carry out a coupled thermal analysis and cope with real technological problems. The coupling is achieved by means of the boundary condition at heat pipe/solid domain interface.
A description of the heat pipe lumped parameter model, suitable for transient as well steady-state analysis, is provided, offering then a brief overview of its potential as a heat pipe design tool. The development of a hybrid solver is presented and the results are compared with a finite element analysis where the heat pipe is simulated as a bar of highly conductive material.
The overall objective of this study is to supply a novel and more comprehensive tool for future heat pipe design and applications, allowing a widespread diffusion thanks to the use of free open source software package. Indeed the hybrid solver is developed in C++ language supported by the finite volume solver OpenFOAM.

Keywords: heat pipe, transient analysis, lumped parameter model, finite volume model, hybrid analysis, OpenFOAM.

List of figures

List of tables

1 Introduction

The heat pipes are two-phase heat transfer devices whose operating principle is based on the evaporation/condensation of a working fluid, and which use the capillary pumping forces to ensure the fluid circulation. They are widely used in space and ground applications mainly because they are able to transfer efficiently large amounts of heat from a heat source (i.e. an external solid component that needs to be cooled) to a heat sink.
The heat pipe performances are generally investigated by lumped parameter models, based on an analogy between the heat pipe operation and an electric network, and widely employed in the literature. From the mathematical viewpoint these models are represented by ordinary differential equations. On the other hand, for the accurate description of the boundary condition of external solid domain at heat pipe interface a distributed approach analysis (i.e. finite volumes or finite elements analysis) is suitable. In the present work, the lumped parameter model and the distributed parameter model are coupled at a numerical level and solved together. In this perspective, boundary conditions on the evaporator section of heat pipe are converted in interface conditions matching the two sub-models. The coupled analysis allows to find the best fit of heat pipe geometrical parameters depending on the external solid domain boundary conditions.
In this chapter the context and the main motivations of this study are explained. A brief overview of the state of the art is also provided.

1.1 Context and motivation

The proposed study will be directly in support of the ESA research project ENCOM-2 (***ENhanced Condensers and related phenOmena in two-phase systeMs***). ENCOM-2 project is developed in order to carry out a thorough investigation in the fields of condensation, heat transfer, two-phase flows and phase transitions.
The main objectives of the ENCOM-2 program are:

- to improve knowledge of the condensation phenomena by means of a theoretical and experimental approach,
- to study the effect of gravity on condensation in order to prove the possibilities of heat transfer enhancement in microgravity,
- to study in deep the physics of phase change of two-phase devices.

The study plan foresees a ground-based experimentation, theoretical studies, numerical modeling and parabolic flights experiments as a preparation to microgravity experiments on ISS (International Space Station).

The aim of this study is to provide a better understanding of heat pipe physical mechanisms and the interaction with heat source solid components. For this purpose a heat pipe lumped parameter model is integrated with a finite volume model in order to carry out a coupled thermal analysis and cope with real technological problems, such as the cooling of electronic in satellites.

The present work package will supply an essential collection of data necessary for the comparison with the experimental data. Numerical modeling will be integrated with experimental investigations as soon as the experimental apparatus will be set up. As the experimental data will become available, they will be used to validate and improve numerical model.

Nevertheless numerical simulations can provide parametric analysis useful to define the role of the main parameters concerning heat pipe design. They can also supply the value of physical variables which are difficult or even impossible to measure since heat pipe is a sealed container. Then the numerical analysis can be useful in planning new experiments. In fact one of the problems in simulating heat pipes is the fact that for very few experimental papers all the characteristics are given, while in this case the numerical activity will be parallel and complementary to the empirical work and all the heat pipe characteristics will be well known before.

It is worthwhile to highlight that, beyond space applications, the heat pipe cooling technology is spreading out for many terrestrial applications detailed in paragraph 2.5. Then the numerical model can be used to optimize heat pipe design for a specific application.

1.2 State of the art

Analyses of the heat pipe operation, both analytical and numerical, have been conducted extensively by many researchers.
Due to the difficulties to find an analytical solution of the heat pipe operation, many numerical models have been developed. The most interesting cover both vapor and liquid flows (e.g., [1], [2], [3], [4], [5]). The heat pipe performances are generally investigated by lumped parameter models. This method has been used in the aerospace industry for about three decades for supporting system-level design analysis.
Another common approach is to model a heat pipe as a bar of highly conductive material. However, that method

- does not simulate a heat pipe's length-independent resistance,
- cannot account for differences in film coefficients between vaporization and condensation,
- can be disruptive to numerical solutions,
- does not provide information on power-length product (for comparison against vendor-supplied heat pipe capacity),
- cannot be extended to include NCG (Non Condensable Gases) effects.

Another misconception is that heat pipes, being two-phase capillary devices, require detailed two-phase thermo-hydraulic solutions. While codes capable of such details exist, such as SINDA/FLUINT, such an approach would represent computational overkill in almost all cases.
A different approach is based on the integration of a heat pipe lumped parameter model with a finite element solver. Lumped and distributed models are numerically coupled in different science fields, mainly in biomedical engineering for numerical modeling of the cardiovascular system.
Quarteroni A. et al. [7] coupled a lumped and a distributed model in order to simulate the complex multi-scale nature of the circulatory system. In particular, a specific district where blood flow behavior is described by the Navier–Stokes equations, is coupled with a lumped model of the remaining part of the circulatory system.
Wenk J.F. et al. [8] presented an approach for modeling the interaction between the heart and the circulatory system. This was accomplished by creating animal-specific biventricular finite element models, which characterize the mechanical response of the heart, and by coupling them

to a lumped parameter model that represents the systemic and pulmonic circulatory system.
Kim H.J. et al. [9] modeled the interactions between the heart and arterial system utilizing a lumped parameter heart model as an inflow boundary condition for three-dimensional finite element simulations of aortic blood flow and vessel wall dynamics.
In this work a hybrid solver is developed integrating an unsteady lumped parameter model in an open source code such as OpenFOAM.
The unsteady lumped parameter model (C. Ferrandi [6]) presented in this study is composed by two lumped models interacting each other, respectively one for the solid components of the heat pipe and the other for the working fluid, circulating inside the device. Most of the physical phenomena which have been neglected in previous models are taken into account and hence a more realistic condition is considered.

2 Heat pipe: basic concepts

This chapter dealt with a literature review in order to investigate the heat pipe operation and design, and transfer limitations. The major advantages over more common heat transfer technologies are highlighted and some examples of the wide range of heat pipe applications are also given.

2.1 Heat pipe operation

The heat pipe is a hollow metal tube that efficiently conducts heat from a heat source (evaporator) to a heat sink (condenser) over relatively long distances (50-500 mm) via the latent heat of vaporization of a working fluid. Therefore it operates by means of a small amount of working fluid contained in a sealed tube, held under a slight vacuum (~10^{-2}Pa). The tube is provided with a wick structure, placed on the inner surface of the heat pipe wall and partially filled with the liquid working fluid.

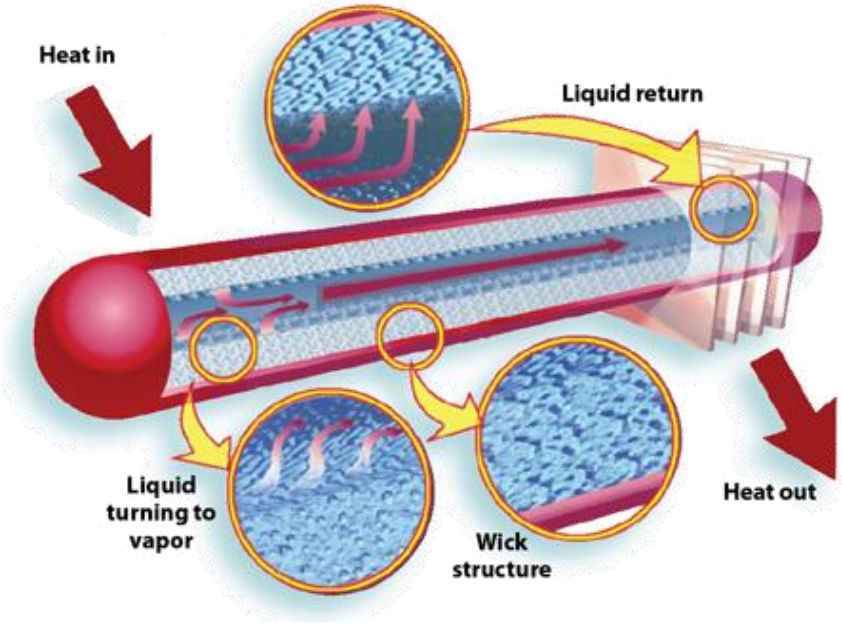

Figure 2.1 Heat pipe operation (courtesy of Thermacore)

Since the container is vacuum sealed, the working fluid is in equilibrium with its own vapor (saturated conditions). With heat addition to one end of the pipe, the working fluid is vaporized as it absorbs an amount of heat equivalent to the latent heat of vaporization, creating a pressure gradient in the pipe. This pressure gradient forces the vapor to flow along the inner channel of the pipe to the cooler section where it condenses, releasing its latent heat of vaporization. The working fluid is then returned to the evaporator by means of the capillary porous wick structure (see Figure 2.1) or by gravity.

The main phenomena characterizing the heat pipe operation are summarized as follows:

- **the vacuum**, that lowers the boiling point of the working fluid, so relatively small increases in temperature vaporize the liquid;
- the **mass addition** in the vapor core of the evaporator section and the mass rejection in the condenser end, that result in a pressure gradient along the vapor channel which drives the corresponding vapor flow;
- the **capillary force**, eventually coupled with **the gravity force**, that acts to return the condensed working fluid back to the hot end of the heat pipe.

The heat pipe is generally divided into three sections: an evaporator section, an adiabatic (or transport) section, and a condenser section. In this regard it is important to highlight that heat pipe is reversible in operation because of its symmetric structure, so the evaporator and condenser sections are identified by the relative position of hot and cold sources. .

Since the latent heat of evaporation is usually very large, considerable quantities of heat can be transferred with a very small temperature difference between the two ends of the pipe. The amount of heat that can be transported as latent heat of vaporization is usually larger than the energy transported by a conventional convective system with an equivalent temperature difference, making the heat pipe more efficient than other competing heat transport technologies.

2.2 Heat pipe design

Heat pipe consists of three basic components:

- the container
- the working fluid
- the wick or capillary structure.

The correct design of the above components is crucial for the optimum operation of the heat pipe.

2.2.1 Container

The container consists of a leak-proof metal tube which provides mechanical support and pressure containment. It must maintain the pressure differential across its walls, and enable transfer of heat to take place from and into the working fluid. The chosen design and processing of the container are extremely important in selecting the metal, because they can affect the useful life of the heat pipe.
Selection of the container material depends on many factors:

- **Thermal conductivity.** A high thermal conductivity ensures minimum temperature drop between the heat source and the wick.
- **Porosity.** The material should be non-porous to prevent the diffusion of vapor.
- **Wettability.**
- **Strength to weight ratio.** A high strength to weight ratio is more important in spacecraft applications.
- Ease of fabrication, including welding, machinability and ductility.
- **Compatibility** both with working fluid and external environment. For heat pipes, working fluid/container compatibility issues encompass any chemical reactions or diffusion processes occurring between the fluid and wall/wick materials that can lead to gas formation and/or corrosion.

2.2.2 Working fluid

One of the key criteria for the selection of a working fluid is the desired operational temperature range. However many other characteristics must be examined in order to determine the most suitable fluid for each different application:

- **High latent heat of vaporization** in order to transfer large amounts of heat power with minimum fluid flow so as to maintain low pressure drops within the heat pipe.
- **High thermal conductivity** in order to minimize the radial temperature gradient and to reduce the possibility of nucleate boiling inside the wick or upon the wall surface.
- Vapor pressure not too high or low over the operating temperature range in order to avoid high vapor velocities and flow instabilities.
- **Low liquid and vapor viscosities** to minimize the resistance to fluid flow.
- **High surface tension** in order to generate a high capillary driving force and operate the heat pipe against gravity.
- Acceptable freezing or pour point.
- Good thermal stability.
- Wettability of wick and wall materials.
- **Compatibility** with wick and wall materials. Table 2.1 lists the compatibilities of several metals and working fluids. Proper container cleaning and heat pipe processing procedures are of extreme importance, since residual contamination within the heat pipe may also lead to gas generation. Steps must also be taken to ensure the purity of the fluid charge; trace amounts of water in ammonia can lead to a reaction with the aluminum container and the formation of hydrogen gas.

Table 2.1 Material compatibility for heat pipe/fluid combination

	Aluminum	Stainless Steel	Copper	Nickel	Titanium
Water	x	✓	✓	✓	O
Ammonia	✓	✓	x	✓	O
Methanol	x	✓	✓	✓	O
Acetone	✓	✓	✓	O	O
Potassium	O	✓	O	✓	x
Sodium	O	O	O	✓	x
✓	Compatible	x	Incompatible	O	Probably compatible

The selection of the working fluid also depends on the various limitations to heat flow occurring within the heat pipe (viscous, sonic, capillary, entrainment and boiling levels) described in paragraph 2.3.

Moreover the working fluid's operational temperature range affects heat pipe's operating limits. A few mediums with their useful ranges of temperature are listed in Table 2.2.

Table 2.2 Working fluids operational range

Fluid	Melting point [°C]	Boiling point at atmospheric pressure [°C]	Useful range [°C]
Helium	-271	-261	-271 to -269
Nitrogen	-210	-196	-203 to -160
Ammonia	-78	-33	-60 to 100
Acetone	-95	57	0 to 120
Methanol	-98	64	10 to 130
Flutec PP2	-50	76	10 to 160
Ethanol	-112	78	0 to 130
Water	0	100	30 to 200
Toluene	-95	110	50 to 200
Mercury	-39	361	250 to 650
Sodium	98	892	600 to 1200
Lithium	179	1340	1000 to 1800
Silver	960	2212	1800 to 2300

2.2.3 Wick

Wick is a porous structure made of materials like steel, aluminum, nickel or copper in various ranges of pore sizes.
The main purpose of the wick is to generate the capillary pressure which is needed to transport the working fluid from the condenser to the evaporator. It must also be able to distribute the liquid around the evaporator section to any area where heat is likely to be received by the heat pipe. Often, depending on various factors (e.g., working fluid, pipe's geometry and orientation) different wick structures are needed to fulfill both the requirements.
The basic features of the wick which must be optimized are listed below:

- **Porosity.** The maximum capillary head generated by a wick increases with decrease in pore size, while the wick permeability increases with increasing pore size.
- **Thickness.** The heat transport capability of the heat pipe is raised by increasing the wick thickness.
- Wettability.
- Compatibility with the working fluid.

Some wick structures are more efficient than others while some have limitations with respect to orientation and gravity.
The most common types of wicks that are used are as follows:

- **Sintered powder.** Wick is made up of sintered metal powder (Figure 2.2). This process provides high power handling, low temperature gradients and high capillary forces for anti-gravity applications. This type of structure allows to achieve very tight bends.

Figure 2.2 Sintered powder heat pipe (courtesy of Thermacore)

- **Screen mesh.** Wick is composed by a multi-layered metal mesh (Figure 2.3). This type of wick is used in the majority of the products (e.g., CPU heat sinks) and provides readily variable characteristics in terms of power transport and orientation sensitivity, according to the number of layers and mesh counts used.

Figure 2.3 Screen mesh heat pipe (courtesy of Thermacore)

- **Grooved tube**. Wick is composed by channels flowing axially on the internal wall of the pipe (Figure 2.4). The small capillary driving force generated by the axial grooves is adequate for low power heat pipes when operated horizontally, or with gravity assistance. The tube can also be bent. When used in conjunction with screen mesh the performance can be considerably enhanced.

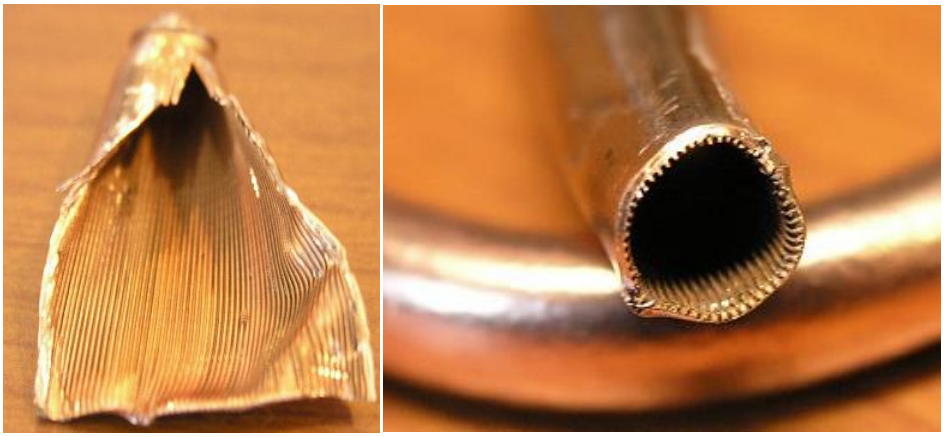

Figure 2.4 Grooved heat pipe (courtesy of Thermacore)

Besides metal wick, fibrous materials like ceramics have also been used widely. They generally have smaller pores. The main disadvantage of ceramic fibers is that, they have little stiffness and usually require a continuous support by a metal mesh. Thus while the fiber itself may be chemically compatible with the working fluids, the supporting materials may cause problems. More recently, interest has turned to carbon fibers as a wick material. Carbon fiber filaments have many fine longitudinal grooves on their surface, have high capillary pressures and are chemically stable. A number of heat pipes that have been successfully built using carbon fiber wicks seem to show a greater heat transport capability.

2.3 Transport limitations

Heat pipe must be tuned depending on the cooling conditions. When heated above a certain temperature, all working fluid in the heat pipe will vaporize and the condensation process will stop. In such conditions, the heat pipe's thermal conductivity is effectively reduced to the heat

conduction properties of its solid metal casing alone. As most heat pipes are constructed of copper (a metal with high heat conductivity), an overheated heat pipe will generally continue to conduct heat at around 1/80 of the original conductivity.
In addition, below a certain temperature, the working fluid will not undergo phase change, and the thermal conductivity will be reduced to that of the solid metal casing. The lower temperature limit typically occurs a few degrees above the freezing point of the working fluid.
Limitations resulting in heat pipe failure are characterized by insufficient liquid flow to the evaporator for a given heat input, thus resulting in dry out of the evaporator wick structure.
The main limitations concerning the maximum heat input are capillary, boiling and entrainment limits.

- **Capillary limit** occurs when the driving capillary pressure is insufficient to provide adequate liquid flow from the condenser to the evaporator, causing dry out of the evaporator wick. Generally, the capillary limit is the primary maximum heat transport limitation of a heat pipe.
- **Boiling limit** occurs when the applied evaporator heat flux is sufficient to cause nucleate boiling in the evaporator wick. This creates vapor bubbles that partially block the liquid return and can lead to evaporator wick dry out.
- **Entrainment limit** refers to the case of high shear forces developed as the vapor passes in the counter flow direction over the liquid saturated wick, where the liquid may be entrained by the vapor and returned to the condenser. This results in insufficient liquid flow to the wick structure.

Other phenomena (e.g., viscous, sonic, condenser limits) cause limited performance loss, increasing the operational temperature of heat pipe.

- **Viscous limit** occurs at low operating temperatures, where the saturation vapor pressure may be of the same order of magnitude as the pressure drop required to drive the vapor flow in the heat pipe. This results in an insufficient pressure available to drive the vapor. The viscous limit is sometimes called the vapor pressure limit.
- **Sonic limit** is due to the fact that at low vapor densities, the corresponding mass flow rate in the heat pipe may result in very high vapor velocities, and the occurrence of choked flow in the vapor passage may be possible.

- **Condenser limit** is based on cooling limitations such as radiation or natural convection at the condenser. For example, in the case of radiative cooling, the heat pipe transport may be governed by the condenser surface area, emissivity, and operating temperature.

Capillary, viscous, entrainment, and sonic limits are axial heat flux limits, that is functions of the axial heat transport capacity along the heat pipe, whereas the boiling limit is a radial heat flux limit occurring in the evaporator.

Limitations can typically be defined in terms of maximum heat flux. More details on this topic are presented in paragraph 4.3.

By evaluating each limitation independently it is possible to determine the heat transport capacity as a function of the mean operating temperature, namely, the adiabatic vapor temperature. The combination of the individual limits yields to detect the heat pipe operational range, defined by the combination of temperatures and maximum transport capacities at which the heat pipe will function (see Figure 2.5). Thus, it is possible to ensure that the heat pipe can transport the required thermal load or to improve the design.

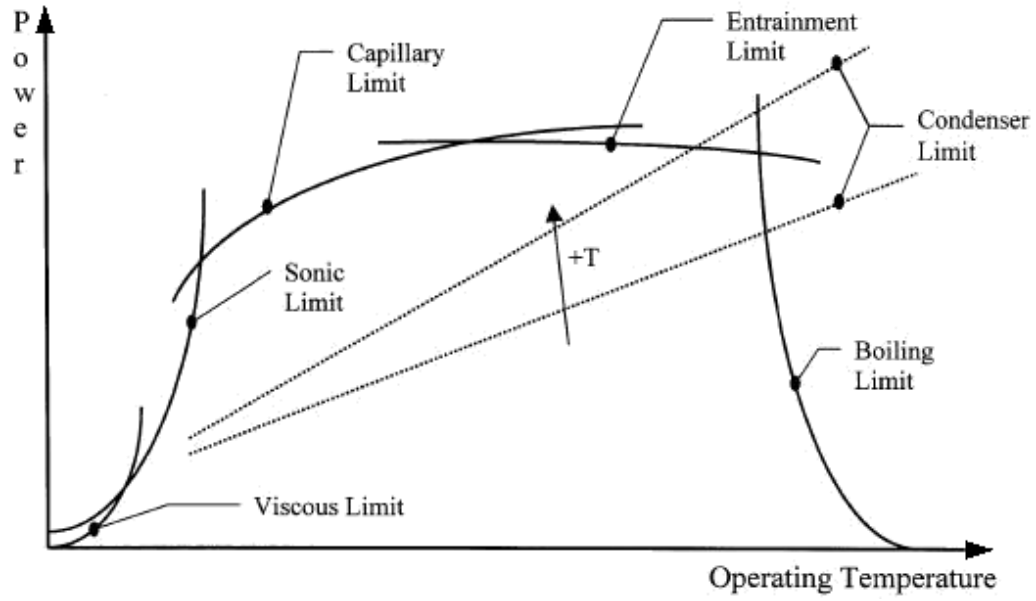

Figure 2.5 Transfer limitations map of heat pipe (courtesy of Ochterback)

2.4 Advantages

Heat pipes offer many distinct advantages over traditional single-phase systems so they are attractive options in a wide range of heat transfer applications. The main features are summarized as follows:

- **Passive device.** They require no external power other than the heat they transfer. They have no moving parts, like mechanical pumps and fans used to circulate the working fluid in traditional systems, which make heat pipes more reliable, free of vibration and completely silent.
- **High thermal capability** associated with the phase change of the working fluid. The amount of heat that can be transported is typically several orders of magnitude greater than single phase systems for a geometrically equivalent system.
- **High heat transfer coefficient.** Thereafter heat pipes can provide essentially isothermal operation regardless of variations in the heat load.
- **Variable thermal conductivity.** Effective thermal conductivity improves with length, and changes with the amount of power being transferred and with the evaporator and condenser sizes.
- Wide range of operating temperatures for working fluids.
- **Low mass flow rates** required to transport equivalent amounts of heat than in single-phase liquid or gas systems for a given temperature range. The thermal capacity of a single-phase system depends on the temperature change of the working fluid; thus, a large temperature gradient or a high mass flow rate is required to transfer a large amount of heat.
- **Small system size and low weight.** As the working fluid operates in a thermodynamic saturated state, the heat pipe then operates in a nearly isothermal condition, which offers benefits of transporting large amounts of heat efficiently, decreasing the overall heat transfer area and saving system weight.
- **Geometrical flexibility.** Heat pipes are manufactured in a multitude of sizes and shapes (see Figure 2.6). If some range of motion is required, they can even be flexible by insertion of a flexible bellows section.
- **Reversibility in operation.** Because of symmetric structure the heat pipe can indistinctly transport heat from one end to the other depending only on the position of heat source, even if it is also

possible to prevent backward heat leak of heat pipes that operate as thermal diodes.

Figure 2.6 Heat pipe of different sizes and shapes

2.5 Applications

Due to the two-phase characteristics, the heat pipe is ideal for transferring heat over long distances (<1m) with a very small temperature drop and for creating a nearly isothermal surface for temperature stabilization.
The use of heat pipes has been mainly limited to space applications until recently, due to cost effectiveness and complex wick construction. Heat pipe cooling technology is currently spreading out for many applications: e.g., cooling electronics, energy recovery, dehumidification enhancement in air conditioning, moulds, medical equipments.

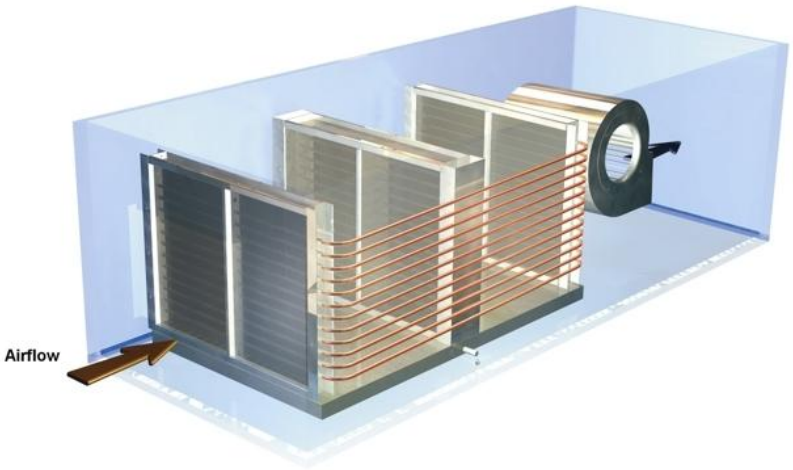

Figure 2.7 Heat pipe for dehumidification systems

Dehumidification and air conditioning. In an air conditioning system, the colder the air as it passes over the cooling coil (evaporator), the more the moisture is condensed out. The heat pipe evaporator resides in the warm incoming stream while the condenser in the cold outgoing stream as shown in Figure 2.7. By transferring heat from the warm return air to the cold supply air, the heat pipes create the double effect of pre-cooling the air before it goes to the evaporator and then re-heating it afterwards. The heat pipe allows the evaporator coil to operate at a lower temperature, increasing the moisture removal capability of the air conditioning system, which results in net energy savings.

Solar water heating system. Solar water heater adopts heat pipe technology which gives high temperature absorption of solar radiation. Highly efficient heat pipe absorbs heat from sunlight and transfers heat to the condenser end. Condenser indirectly contacts with water through a copper cap releasing the heat gained from vacuum tube. (Figure 2.8).

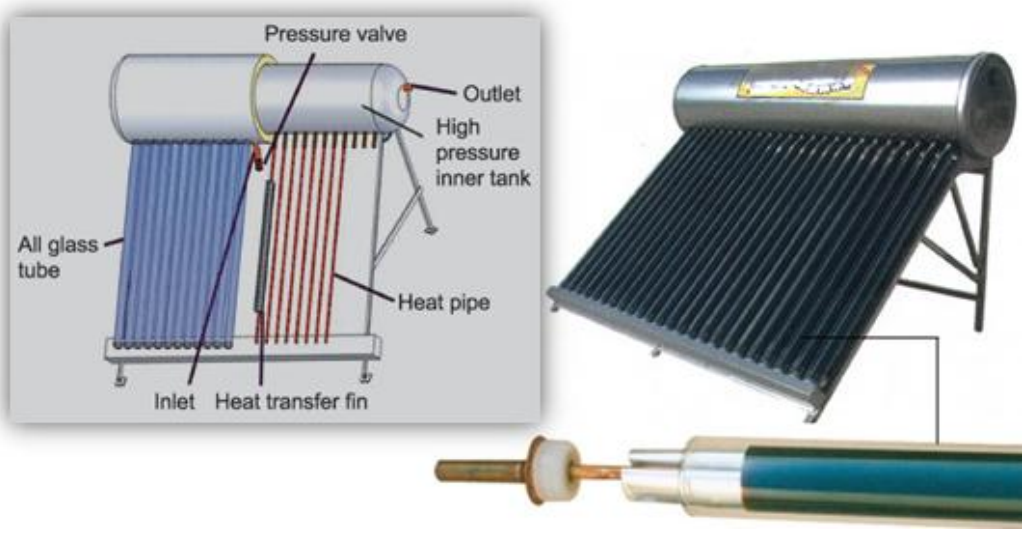

Figure 2.8 Heat pipe integrated pressurized solar water heater

Injection moulds and die casting dies. Heat pipes are widely used for improving cooling efficiency of injection moulds and Die casting dies. This cooling method helps reduce cycle time and rejection, eliminate hot spots, improve quality of products, and is very useful when only limited space is available for providing channels for water-cooling, traditionally used in these applications. Furthermore, effectiveness of water cooling decreases in conventional systems due to rusting, blocking of cooling channels; while using heat pipes, since water is not circulated directly in

the core (see Figure 2.9), cooling efficiency remains the same throughout the life of the mould.

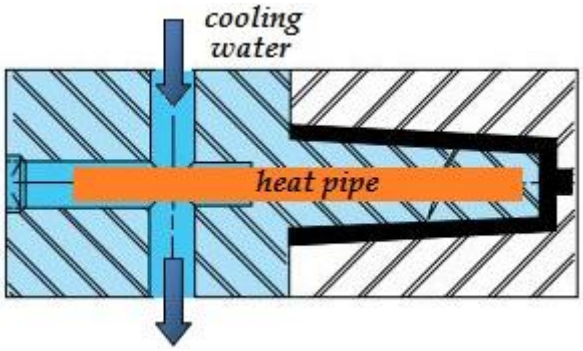

Figure 2.9 Sketch of heat pipe in mould embedded

Electronics. Heat pipe has been applied to laptop computer cooling since it is an ideal, cost effective solution. Its light weight (generally less than 40 grams), small, compact profile, and its passive operation, allows to meet the demanding requirements of laptops.

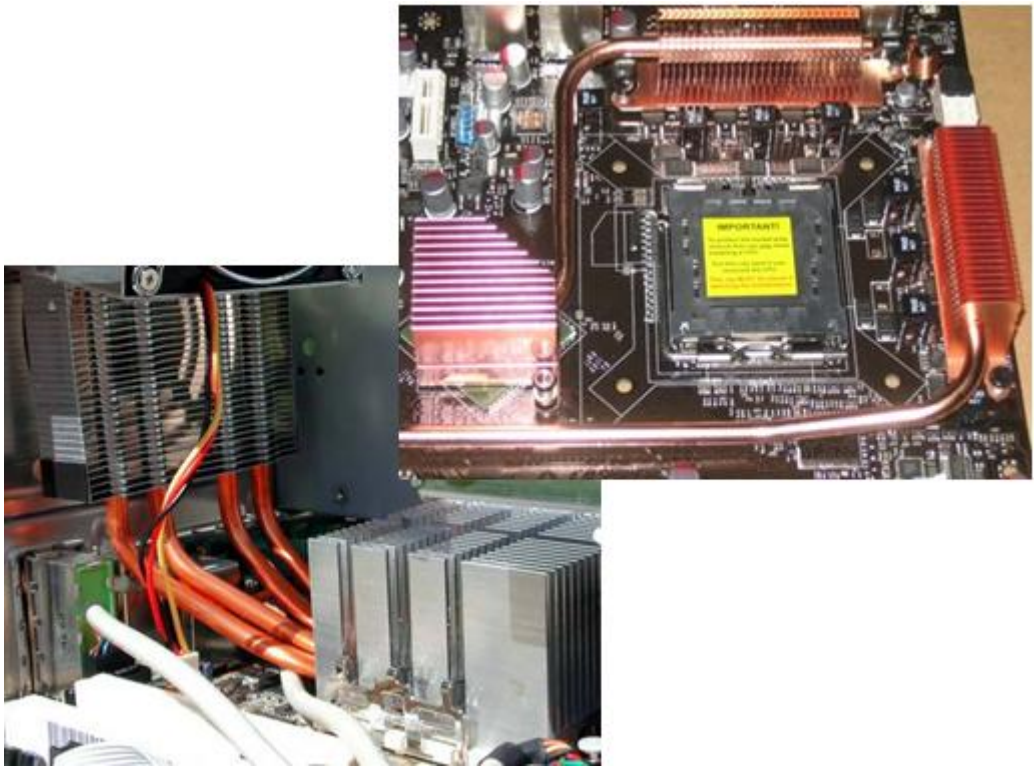

Figure 2.10 Heat pipes designed to direct the heat from the chipsets to the heat sink, where it can be carried away by airflow from a fan

One end of the heat pipe is attached to the processor with a thin, clip-on mounting plate. The other is attached to the heat sink: e.g., a specially designed keyboard RF shield, cooling fins, a fan (Figure 2.10).

Space technology. Heat pipes are good candidates in thermal transfer in space applications. Heat transfer by means other than the heat pipe can have the following impacts:

- a price paid with respect to weight and size of the heat transfer equipment,
- significant heat loss in transfer over considerable distances,
- electromotive devices, such as liquid pumps, required to move the heat,
- possible problems presented by operation in zero gravity.

Actual heat pipes used in spacecraft applications operate between 200 K and 350 K. Consequently, a working fluid whose freezing and boiling points encompass this temperature range and has a high latent heat, a low viscosity, and high heat transport capability must be selected. Ammonia is an appropriate working fluid whose fluid properties meet these criteria. However, for safety reasons, the toxicity of ammonia precludes its use in manned environments. Aluminum alloys are suitable for the container material of the heat pipe because of their long-term compatibility with ammonia, heritage, good thermal compatibility with aluminum radiators and heat sinks, and weldability characteristics. For long-term space missions, methanol and water exhibit an incompatibility with aluminum, and should not be used.

Though heat pipes are reliable systems, their usage involves some risks. Improper cleaning and processing of the aluminum container could result in contaminants reacting with the ammonia to form a small quantity of non-condensable gas, which will interfere with the flow of vapor and reduce the heat transfer effectiveness. Contaminants reacting with ammonia normally produce hydrogen, and the gas collects in the condenser region. As more and more of the condenser is blocked, the surface area available for heat rejection decreases, reducing the heat transfer effectiveness; ultimately, the heat pipe may cease to function. Failure to certify welds at the end caps and the fill tube could result in improper or defective welds permitting leaks or catastrophic failure of the pressure vessel.

3 Lumped parameter model

*T*his chapter presents the lumped parameter model of the heat pipe composed by two electrical circuits interacting each other, respectively one for the solid components and the other one for the working fluid circulating inside the device. More specifically, the model refers to a cylindrical sintered heat pipe. The main novelty of this model is the solid/fluid thermal coupling neglected in previous studies available from the literature. The present model has been defined starting from a previous work (C. Ferrandi [10]) and then improved correcting minor flaws. In this form the model has been considered for a journal paper and submitted to Heat Transfer Engineering Journal.

3.1 Introduction

The heat pipe operation is described by a lumped parameter model based on the electrical analogy. Solid components and fluidic domains are subdivided into a number of finite sub-volumes, called nodes or lumps. The thermal properties and the average temperature of each sub-volume are assumed to be concentrated in the relative node. Nodes are connected to each other by means of resistive, capacitive and inductive elements modeling different physical phenomena namely thermal or flow resistance, thermal inertia or fluid inertia. Thus the physical system is reduced to an electrical network where the current and the tension represent respectively the thermal flux and the temperature difference between two nodes. Appling Ohm's law and Kirchhoff's law it is possible to obtain an ordinary differential equation governing each node, so the overall transient problem can be reduced to a linear system of ODE easily implemented in a code and numerically solved.

3.2 Solid region network

The solid region consists of two domains: the pipe wall and the wick structure. Each domain is subdivided into three nodes (i.e., evaporator, adiabatic and condenser sections) representing the mid-wall temperatures. Six different nodes (T_{pe}, T_{pa}, T_{pc}, T_{we}, T_{wa}, T_{wc}) have been identified in Figure 3.1. They are connected by means of resistances and capacitors. The properties of each node are identified by a subscripts with two letters: the first one refers to the domains, so *p* stands for pipe wall and *w* for wick, the second one refers to the three sections, so *e* stands for evaporator, *a* for adiabatic zone and *c* for condenser.
T_{eva} and T_{cond} are the average outer wall temperatures of the evaporator and condenser (boundary conditions), while T_{ve} and T_{vc} represent the vapor temperatures calculated in the fluidic model described in the paragraph 3.3.

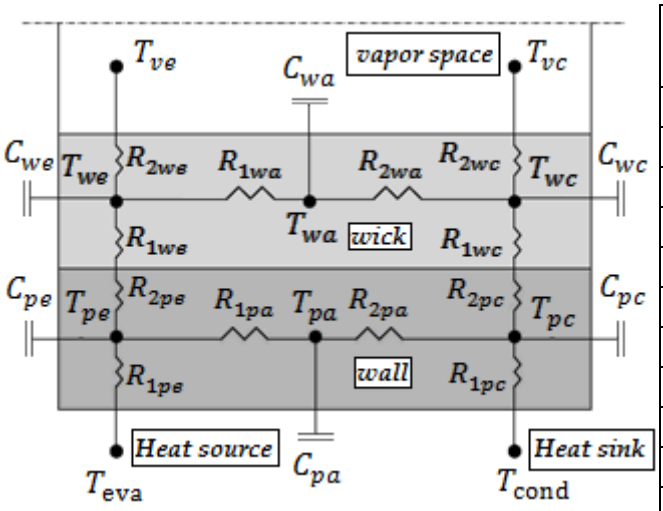

Figure 3.1 Solid network

Symbol	Section, Domain	Type
R_{pe}	Evap., wall	Rad. Resist.
R_{we}	Cond., wick	Rad. Resist.
R_{pa}	Adiab., wall	Ax. Resist.
R_{wa}	Adiab., wick	Ax. Resist.
R_{pc}	Cond., wall	Rad. Resist.
R_{wc}	Cond., wick	Rad. Resist.
C_{pe}	Evap., wall	Capacitor
C_{we}	Cond., wick	Capacitor
C_{pa}	Adiab., wall	Capacitor
C_{wa}	Adiab., wick	Capacitor
C_{pc}	Cond., wall	Capacitor
C_{wc}	Cond., wick	Capacitor

According to the electrical analogy, the radial and the axial heat conduction in the heat pipe solid components can be modeled as thermal resistances with the following formulas valid for a cylindrical geometry.

$$R_{\text{radial}} = \frac{\ln(r_{\text{ext}}/r_{\text{int}})}{2\pi kL} \qquad (3.1)$$

$$R_{axial} = \frac{L}{kA} \tag{3.2}$$

r_{ext} and r_{int} are the external and internal radius, A and L are respectively the cross sectional area and the length of the sub-domain, k is the thermal conductivity. For solid wall k is the thermal conductivity of the pure material, while for the wick it is necessary to determine an effective conductivity (k_{eff}) that takes into account the thermal conductivity of both liquid and metal. The code implements the following three correlations:

- **wrapped screen week**

$$k_{eff} = \frac{k_l[(k_l + k_w) - (1-\varepsilon)(k_l - k_w)]}{[(k_l + k_w) + (1-\varepsilon)(k_l - k_w)]} \tag{3.3}$$

- **Packed sphere wick**

$$k_{eff} = \frac{k_l[(2k_l + k_w) - 2(1-\varepsilon)(k_l - k_w)]}{[(2k_l + k_w) + (1-\varepsilon)(k_l - k_w)]} \tag{3.4}$$

- **Sintered wick**

$$k_{eff} = \frac{k_l[(2 + k_l/k_w) - 2\varepsilon(1 - k_l/k_w)]}{[(2 + k_l/k_w) + \varepsilon(1 - k_l/k_w)]} \tag{3.5}$$

k_l and k_w are the thermal conductivities respectively of liquid and of wick material and ε is the wick porosity.
Thermal inertia of each heat pipe section is modeled as a thermal capacity:

$$C = \rho c V \tag{3.6}$$

where C is thermal capacity, ρ is the density of material, c is the specific heat of material and V is the volume of the sub-domain. As for the wick thermal resistance an effective thermal capacity must be estimated:

$$C = (\rho c)_{eff} V \tag{3.7}$$

where

$$(\rho c)_{eff} = \varepsilon(\rho c)_l + (1-\varepsilon)(\rho c)_w \tag{3.8}$$

Referring to Figure 3.2, incoming heat power to node i from node j can be determined as follows

$$\dot{Q}_{ij} = -\frac{T_i - T_j}{R_{ij}} \tag{3.9}$$

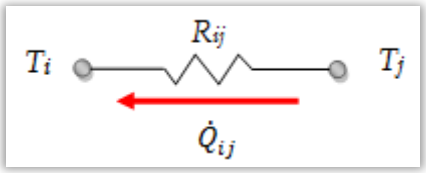

Figure 3.2 Electrical analogy in thermal analysis

The general transient heat conduction equation governing each solid node (T_{pe}, T_{pa}, T_{pc}, T_{we}, T_{wa}, T_{wc}) is:

$$C_i \frac{dT_i}{dt} = \sum_{j=1,j\neq 1}^{N} \dot{Q}_{ij} \tag{3.10}$$

where N is the number of nodes electrically connected to node i by resistance R_{ij}.

3.3 Fluidic network

Fluid motion is governed by continuity equations of mass and momentum, which have been reduced to ordinary differential or algebraic equations (necessary to build the electric network) thanks to the following fundamental assumptions:

1. Fluid path is one-dimensional.
2. Liquid is incompressible.
3. Vapor is represented by the ideal gas equations.
4. Vapor expansion and compression are polytropic processes.
5. Flow is laminar for both vapor and liquid.
6. Evaporation and condensation phenomena are confined respectively in the evaporator and in the condenser zones.
7. Liquid mass flow rate is constant in the wick adiabatic section.
8. Liquid temperature is equal to the wick temperature in each heat pipe section.

The vapor domain has been subdivided into three sections: two *vapor tanks* and one *vapor path* connecting the two tanks, where the vapor mass ($\dot{m}_v$) travels in the axial direction driven by the pressure difference between the evaporator and the condenser.
The same scheme is adopted for the liquid: two *liquid tanks* accounting for the liquid storage in the wick and a *liquid path* modeling the liquid mass ($\dot{m}_l$) flowing from the condenser back to the evaporator zone through the porous wick in the adiabatic section.
Additionally the vapor and liquid tanks are connected by means of two more fluidic paths representing pressure drops at the liquid/vapor interface in the evaporator and condenser sections respectively. A sketch of fluidic model is illustrated in Figure 3.3.

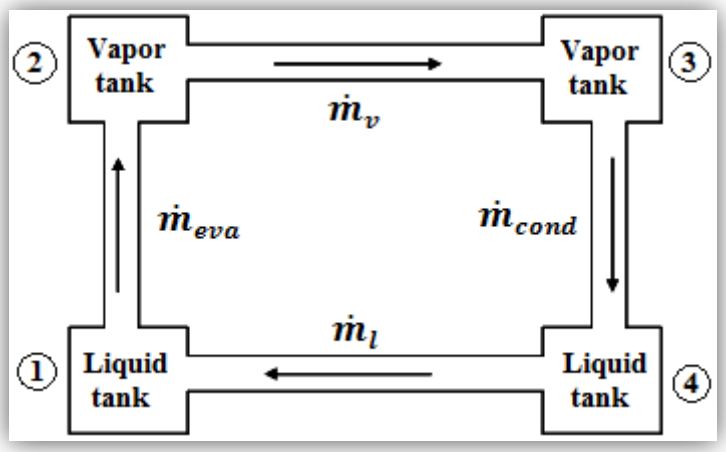

Figure 3.3 Fluidic model

The fluid cycle may be resumed in the following four steps:

a. The liquid tank in the evaporator zone (1) is heated up; a mass of vapor ($\dot{m}_{\mathrm{eva}}$) is produced and flows into the vapor tank (2).
b. Pressure increases inside the vapor tank (2) and a mass of vapor ($\dot{m}_v$) is pushed in the condenser vapor tank (3) through the vapor path.
c. The condenser zone is cooled down; a mass of fluid ($\dot{m}_{\mathrm{cond}}$) is condensed and flows into the condenser liquid tank (4).
d. The wick capillary pressure pushes a mass of liquid ($\dot{m}_l$) from the condenser liquid tank (4) back to the evaporator liquid tank (1) through the liquid path.

Governing equations related to each process are clearly defined in the next paragraphs.

3.3.1 Vapor tank

Assuming vapor inside tanks as an ideal gas,

$$\frac{\partial p_v}{\partial \rho_v} = \gamma R^* T_v \tag{3.11}$$

the mass continuity equation

$$V_v \frac{\partial \rho_v}{\partial t} = \sum \dot{m}_v \tag{3.12}$$

can be rewritten as follows for the evaporator

$$\frac{V_{ve}}{\gamma R^* T_{ve}} \frac{\partial P_{ve}}{\partial t} = \dot{m}_{\text{eva}} - \dot{m}_v \tag{3.13}$$

where $\dot{m}$ is the mass flow rate, p is the pressure, R^* is the vapor perfect gas constant, t is time, V is the tank volume, T is the temperature of the vapor in the tank, and γ is the polytropic exponent.
Defining the flow capacitance as

$$C_{ve} = \frac{V_{ve}}{\gamma R^* T_{ve}} \tag{3.14}$$

the differential equation can be rewritten as follows

$$C_{ve} \frac{\partial P_{ve}}{\partial t} = \dot{m}_{\text{eva}} - \dot{m}_v \tag{3.15}$$

In the condenser the mass continuity equation is similar:

$$C_{vc} \frac{\partial P_{vc}}{\partial t} = \dot{m}_v - \dot{m}_{\text{cond}} \tag{3.16}$$

Vapor temperature is linked to pressure by the adiabatic polytropic equation

$$T p^{\frac{1-\gamma}{\gamma}} = constant \tag{3.17}$$

that can be derived obtaining the following relations for the evaporator and the condenser:

$$\frac{\partial T_{ve}}{\partial t} = \frac{\gamma - 1}{\gamma} \frac{T_{ve}}{p_{ve}} \frac{dp_{ve}}{dt}$$
$$\frac{\partial T_{vc}}{\partial t} = \frac{\gamma - 1}{\gamma} \frac{T_{vc}}{p_{vc}} \frac{dp_{vc}}{dt} \tag{3.18}$$

Mass flow rates in the evaporation and condensation processes are relatively estimated as follows

$$\dot{m}_{\text{eva}} = \frac{\dot{Q}_{\text{eva}}}{h_{lv}} \qquad \dot{m}_{\text{cond}} = \frac{\dot{Q}_{\text{cond}}}{h_{lv}} \tag{3.19}$$

where $\dot{Q}$ is the heat power throughput and h_{lv} is the latent heat of vaporization/condensation.
For the present numerical simulations it is also assumed an adiabatic process for the vapor flow, i.e. the heat capacity ratio is defined as follows

$$\gamma(T_v) = \frac{c_p(T_v)}{c_v(T_v)} \tag{3.20}$$

3.3.2 Vapor duct

The one-dimensional momentum equation for laminar flow is

$$\rho \frac{\partial u}{\partial t} - \mu \frac{\partial^2 u}{\partial^2 x} + \frac{\partial p}{\partial x} = 0 \tag{3.21}$$

Integrating on the effective duct length L_{eff}

$$L_{\text{eff}} = \frac{L_{\text{eva}}}{6} + L_a + \frac{L_{\text{cond}}}{6} \tag{3.22}$$

the eq. 3.21 reduces as follows:

$$\int_{L_{\text{eff}}} \left(\rho \frac{\partial u}{\partial t} - \mu \frac{\partial^2 u}{\partial^2 x} + \frac{\partial p}{\partial x} \right) dl = 0 \tag{3.23}$$

Assuming constant fluid properties in time and space, each term of eq. 3.23 can be developed as follows:

$$\int_{L_{\text{eff}}} \rho \frac{\partial u}{\partial t} dl = \rho_{va} L_{\text{eff}} \frac{du}{dt} = \frac{L_{\text{eff}}}{\pi r_{iw}^2} \frac{d\dot{m}_v}{dt} = \bar{L}_{va} \frac{d\dot{m}_v}{dt} \tag{3.24}$$

$$\begin{aligned} \int_{L_{\text{eff}}} \mu \frac{\partial^2 u}{\partial^2 x} dl &= \rho_{va} \frac{64}{Re} \frac{L_{\text{eff}}}{\pi r_{iw}} \frac{u^2}{2} \\ &= \rho_{va} \frac{64 \mu_{va}}{2 r_{iw} \rho_{va} u} \frac{L_{\text{eff}}}{\pi r_{iw}} \frac{u^2}{2} \\ &= \frac{8 \mu_{va}}{\rho_{va}} \frac{L_{\text{eff}}}{\pi r_{iw}^2} \dot{m}_v = \bar{R}_{va} \dot{m}_v \end{aligned} \tag{3.25}$$

$$\int_{L_{\text{eff}}} \frac{\partial p}{\partial x} dl = p_{vc} - p_{ve} \tag{3.26}$$

Rearranging eq.s 3.24, 3.25, 3.26 yields the following equation:

$$\bar{L}_{va} \frac{d\dot{m}_v}{dt} = \bar{R}_{va} \dot{m}_v + p_{ve} - p_{vc} \tag{3.27}$$

where $\bar{L}_{va}$ and $\bar{R}_{va}$ represent, respectively, the vapor flow inductance and resistance.

3.3.3 Liquid tank

Applying the conservation of mass to each liquid tank gives the following equation for evaporator and condenser:

$$\begin{aligned} \frac{dM_{lc}}{dt} &= \dot{m}_{\text{cond}} - \dot{m}_l \\ \frac{dM_{le}}{dt} &= \dot{m}_l - \dot{m}_{\text{eva}} \end{aligned} \tag{3.28}$$

where

$\dot{m}_{\text{cond}}$ *and* $\dot{m}_{\text{eva}}$ are the mass flow rates in the evaporation and condensation processes;

$\dot{m}_l$ is the mass flow rate in the liquid duct;

M_{lc} and M_{le} are respectively the liquid mass in the wick volume of condenser and of evaporator, calculated as follows:

$$M_{lc} = \rho_{lc}\varepsilon\pi(r_{ew}^2 - r_{iw}^2)L_{\text{cond}}$$
$$M_{le} = \rho_{le}\varepsilon\pi(r_{ew}^2 - r_{iw}^2)L_{\text{eva}} \quad (3.29)$$

3.3.4 Liquid duct

The liquid flow inside the porous medium is modeled with the Darcy equation:

$$\nabla p = -\frac{\mu}{K}\text{u} \quad (3.30)$$

where

K is the porous wick permeability

u is the Darcy flux, which is related to the velocity of fluid traveling through the pores by the porosity.

$$\text{u} = \frac{u_l}{\varepsilon} \quad (3.31)$$

Equation 3.31 account for the fact that only a fraction of the total volume of wick is available for flow.

Being the evaporation and condensing process limited to the storage tanks, the liquid duct is arranged as a pure resistive element where the fluid velocity is constant and the liquid mass flow rate is estimated as

$$\dot{m}_{la} = \rho_{la}\varepsilon\pi(r_{ew}^2 - r_{iw}^2)\text{u} \quad (3.32)$$

Substituting the eq. 3.32 in eq. 3.30 and integrating on the adiabatic section length L_a, gives the equation:

$$\frac{\mu_{la}L_a}{K\rho_{la}\varepsilon\pi(r_{ew}^2 - r_{iw}^2)}\dot{m}_{la} = \bar{R}_{la}\dot{m}_{la} = p_{lc} - p_{le} \quad (3.33)$$

In analogy with eq. 3.27, $\bar{R}_{la}$ is the liquid flow resistance.

The permeability K is estimated using empirical correlations derived from literature and depending on the wick grains radius r_g, such as the empirical law reported below (K.C. Leong [14]):

$$K = \frac{4r_g^2\varepsilon^2}{150(1-\varepsilon)^2} \tag{3.34}$$

The complete fluidic electrical scheme is reported in Figure 3.4.

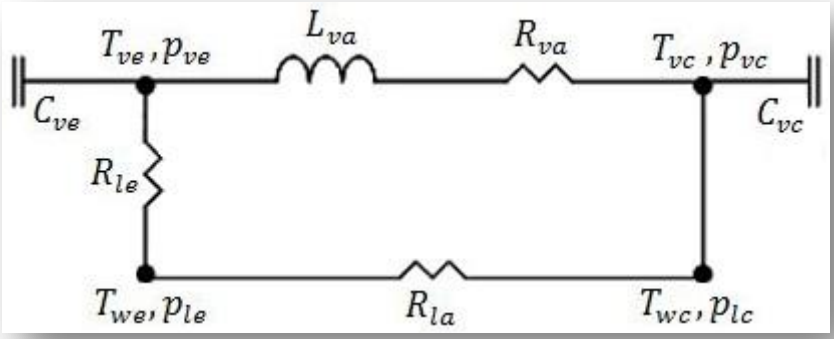

Figure 3.4 Fluidic network

3.3.5 Liquid/vapor coupling

As vaporization occurs in the evaporator, the liquid meniscus recedes correspondingly into the wick structure. Similarly, as vapor condenses in the condenser region, the mass addition results in an advanced meniscus, see Figure 3.5a . The difference between the capillary radii in the evaporator and condenser ends of the wick structure results in a net pressure difference in the liquid-saturated wick. This pressure difference drives the liquid from the condenser through the wick structure to the evaporator region, thus allowing the overall process to be continuous.
The capillary pressure difference sustained across the interface between liquid and vapor due to surface tension is described by Young-Laplace equation:

$$\Delta p_{vl} = \frac{2\sigma}{r_c} \tag{3.35}$$

where

Δp_{vl} is the pressure difference at liquid/vapor interface,
r_c is the capillary radius,
σ is the surface tension.

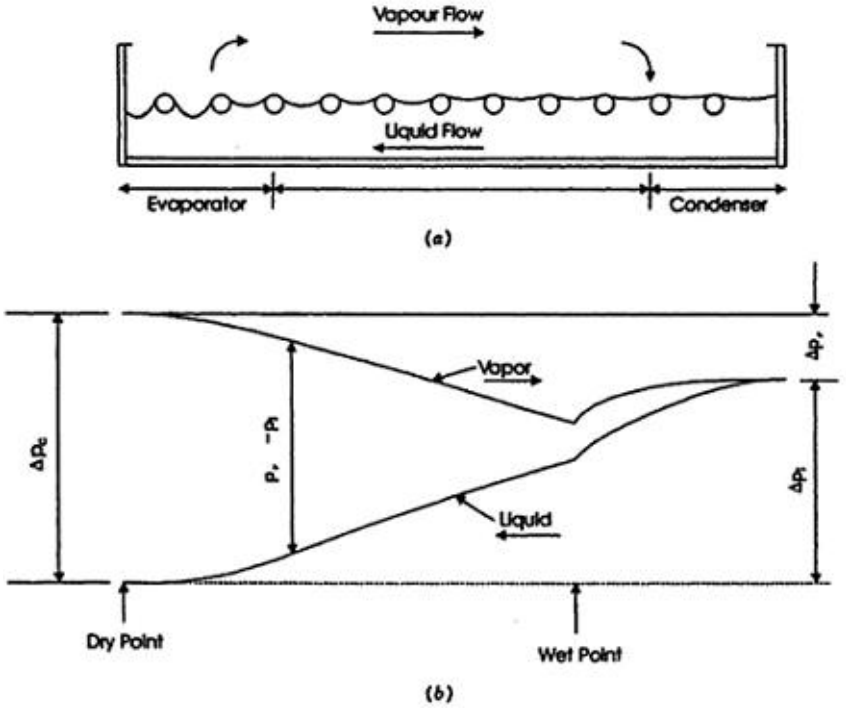

Figure 3.5 Pressure fluid profile (courtesy of Rosenfeld)

According to S.W. Chi [12] the capillary radius of a packed sphere wick is estimated as follows:

$$r_c = 0.41\, r_g \tag{3.36}$$

where r_g is the sphere radius.
Small capillary radii, typical of the evaporator section, lead to important pressure differences between the two phases, while capillary pressure may be negligible in the condenser. Figure 3.5b shows the typical liquid and vapor pressure trends along the heat pipe length.
Thereafter, neglecting capillary pressure difference in the condenser section ($p_{vc} = p_{lc}$) and determining p_{ve} from eq. 3.15, it is possible to calculate the pressure of liquid at the evaporator section p_{le} by the following equation:

$$p_{ve} - p_{le} = f\frac{2\sigma}{r_c} \tag{3.37}$$

where a correction coefficient f accounts for the influence of the wick dry-out on the pressure drop Δp. The correction coefficient is calculated as follows:

$$f = -\left(\frac{M_e}{M_{e0}}\right) + 1 \qquad if\ 0 \le M_e \le M_{e0}$$
$$f = \frac{p_{ve} - p_{vc}}{\frac{2\sigma}{r_c}} \qquad if\ M_e > M_{e0} \tag{3.38}$$

where Me_0 is the maximum liquid mass capability of the evaporator wick:

$$M_{e0} = \rho_{le}\varepsilon\pi(r_{ew}^2 - r_{iw}^2)L_{\text{eva}} \tag{3.39}$$

At the beginning of the simulation the porous wick in the evaporator is assumed saturated of liquid. The evaporation causes a reduction of the amount of liquid, therefore the pressure p_{le} decreases faster than expected because of the increase of the sucking pressure of the evaporator with respect to the condenser.
In case of complete dryness of the evaporator wick p_{le} reaches its minimum value with the strongest drain of the liquid from the condenser (see Figure 3.6).

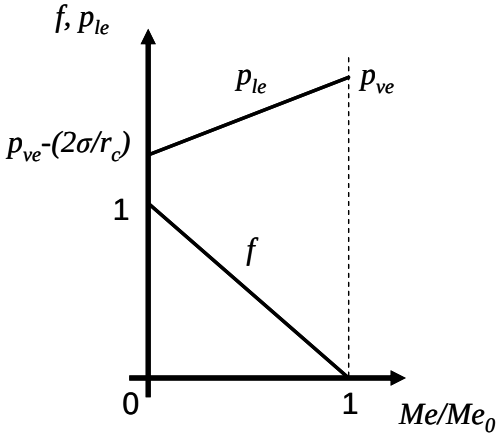

Figure 3.6 f and p_{le} variation at $Me/Me0$ variation

3.3.6 Solid/fluid thermal coupling

Coupling of solid and fluidic networks is achieved by equations 3.19, where heat powers are rewritten in terms of thermal resistances.

$$\dot{Q}_{\text{eva}} = \frac{T_{we} - T_{ve}}{R_{2we}}$$
$$\dot{Q}_{\text{cond}} = -\frac{T_{wc} - T_{vc}}{R_{2wc}} \tag{3.40}$$

Then evaporation and condensation mass flow rates are written as a function of temperatures:

$$\dot{m}_{\text{eva}} = \frac{T_{we} - T_{ve}}{R_{2we}\, h_{lv}}$$
$$\dot{m}_{\text{cond}} = -\frac{T_{wc} - T_{vc}}{R_{2wc}\, h_{lv}} \tag{3.41}$$

It is also worthwhile to remember that the liquid temperature is assumed to be equal to the wick temperature in each heat pipe section:

$$T_{we} = T_{le}$$
$$T_{wc} = T_{lc} \tag{3.42}$$

3.4 Complete system of equations and boundary conditions

The system of first-order, linear, ordinary differential equations governing heat pipe transient operation is:

$$\begin{cases} C_{pe}\dfrac{dT_{pe}}{dt} = \dot{Q}_{\mathrm{IN}} - \dfrac{T_{pe}-T_{pa}}{R_{1pa}} - \dfrac{T_{pe}-T_{we}}{R_{2pe}+R_{1we}} \\ C_{pc}\dfrac{dT_{pc}}{dt} = -\dfrac{T_{pc}-T_{pa}}{R_{2pa}} - \dfrac{T_{pc}-T_{wc}}{R_{2pc}+R_{1wc}} - \dfrac{T_{pc}-T_{f}}{R_{1pc}+R_{f}} \\ C_{we}\dfrac{dT_{we}}{dt} = -\dfrac{T_{we}-T_{wa}}{R_{1wa}} + \dfrac{T_{pe}-T_{we}}{R_{2pe}+R_{1we}} - \dfrac{T_{we}-T_{ve}}{R_{2we}} \\ C_{wc}\dfrac{dT_{wc}}{dt} = -\dfrac{T_{wc}-T_{wa}}{R_{2wa}} + \dfrac{T_{pc}-T_{wc}}{R_{2pc}+R_{1wc}} - \dfrac{T_{wc}-T_{vc}}{R_{2wc}} \\ C_{pa}\dfrac{dT_{pa}}{dt} = -\dfrac{T_{pa}-T_{pe}}{R_{1pa}} - \dfrac{T_{pa}-T_{pc}}{R_{2pa}} \\ C_{wa}\dfrac{dT_{wa}}{dt} = -\dfrac{T_{wa}-T_{we}}{R_{1wa}} - \dfrac{T_{wa}-T_{wc}}{R_{2wa}} \\ \bar{L}_{va}\dfrac{d\dot{m}_{v}}{dt} = \bar{R}_{va}\dot{m}_{v} + p_{ve} - p_{vc} \\ C_{ve}\dfrac{\partial P_{ve}}{\partial t} = \dfrac{T_{we}-T_{ve}}{R_{2we}\,h_{lv}} - \dot{m}_{v} \\ C_{vc}\dfrac{\partial P_{vc}}{\partial t} = \dot{m}_{v} - -\dfrac{T_{wc}-T_{vc}}{R_{2wc}\,h_{lv}} \\ \dfrac{\partial T_{ve}}{\partial t} = \dfrac{\gamma-1}{\gamma}\,\dfrac{T_{ve}}{p_{ve}}\,\dfrac{dp_{ve}}{dt} \\ \dfrac{\partial T_{vc}}{\partial t} = \dfrac{\gamma-1}{\gamma}\,\dfrac{T_{vc}}{p_{vc}}\,\dfrac{dp_{vc}}{dt} \\ \dfrac{dM_{le}}{dt} = \dfrac{P_{vc}-P_{ve}}{\bar{R}_{va}} + \dfrac{2\sigma f}{\bar{R}_{va}r_{c}} - \dfrac{T_{we}-T_{ve}}{R_{2we}\,h_{lv}} \\ \dfrac{dM_{lc}}{dt} = -\dfrac{T_{wc}-T_{vc}}{R_{2wc}\,h_{lv}} - \dfrac{P_{vc}-P_{ve}}{\bar{R}_{va}} - \dfrac{2\sigma f}{\bar{R}_{va}r_{c}} \end{cases} \tag{3.43}$$

The unknown vector is

$$\boldsymbol{y} = \left\{T_{pe}\; T_{pc}\; T_{we}\; T_{wc}\; T_{pa}\; T_{wa}\;\; \dot{m}_{v}\;\; P_{ve}\; P_{vc}\; T_{ve}\; T_{vc}\; M_{le}\; M_{lc}\right\}^{T} \tag{3.44}$$

The system of equation 3.43 and the initial conditions for **y** are summarized here below in form of Cauchy's problem.

$$\begin{cases} \dfrac{d\boldsymbol{y}}{dt} = \boldsymbol{f}(t, \boldsymbol{y}) \\ \boldsymbol{y}(t_0) = \boldsymbol{y_0} \end{cases} \tag{3.45}$$

Applying a general numerical integration method (details are given in paragraph 4.2), the system of ordinary equations turns into a system of linear equations.

$$\underline{\boldsymbol{A}}\,\boldsymbol{y} = \boldsymbol{b} \tag{3.46}$$

Once the initial and boundary conditions are defined, the system can be numerically solved.
The boundary conditions, which can be either isoflux, isothermal or convective, are applied independently in the evaporator and condenser regions as better explained hereafter.

3.4.1 Evaporator section boundary conditions

Concerning the evaporator section two kinds of boundary conditions have been considered:

- **Dirichlet boundary condition**. A constant temperature value of T_{eva} can be imposed defining the input thermal power as follows (see solid network scheme in Figure 3.1)

$$\dot{Q}_{IN} = -\frac{T_{pe} - T_{\text{eva}}}{R_{1pe}} \tag{3.47}$$

  and substituting the expression in the first equation of system 3.43.
- **Neumann boundary condition,** that is a constant or variable heat power input $\dot{Q}_{\text{IN}}$ imposed on the external surface of pipe.

3.4.2 Condenser section boundary conditions

Concerning the condenser section the following boundary conditions have been modeled:

- **Dirichlet boundary condition**, that is a constant temperature T_{cond}. Referring to the second equation of system 3.43 and the solid network scheme of Figure 3.1, the boundary condition can be expressed as

$$T_f = T_{\text{cond}}$$
$$R_f = 0 \tag{3.48}$$

- **Robin boundary condition,** that is a convective condition defining the outgoing power heat $\dot{Q}_{\text{conv}}$ as follows (see Figure 3.7)

$$\dot{Q}_{\text{conv}} = -\frac{T_{pc} - T_f}{R_{1pc} + R_f} \tag{3.49}$$

where T_f is the cooling medium temperature and R_f is the convective thermal resistance. Thence a new thermal resistance must be added to the thermal network, as shown in Figure 3.7:

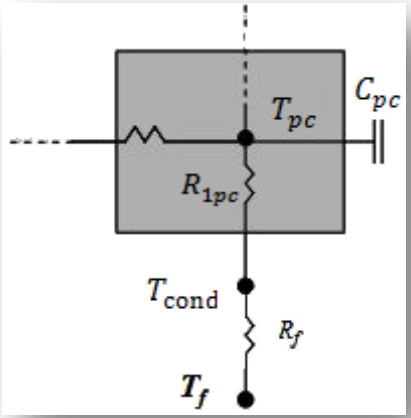

Figure 3.7 Convective boundary condition scheme

$$R_f = \frac{1}{h_f A_f} \tag{3.50}$$

where A_f is the external surface of condenser section and h_f is the convective heat transfer coefficient.
If the latter is unknown it is possible to define the mass flow rate $\dot{m}_f$ of the cooling medium and then estimate the cooling heat transfer coefficient h_f by means of the following correlation:

$$Nu = \frac{h_f D_f}{k_f} = C\,\mathrm{Re}^m\,\mathrm{Pr}^{1/3} = C\left(\frac{\dot{m}_f}{\mu_f}\frac{D_f}{A_f}\right)^m\left(\frac{c_f \mu_f}{k_f}\right)^{1/3}$$

$$\begin{cases} C = 0.989 & \text{m=0.33} & 0.4 \le \mathrm{Re} \le 4 \\ C = 0.911 & \text{m=0.385} & 4 \le \mathrm{Re} \le 40 \\ C = 0.683 & \text{m=0.466} & 40 \le \mathrm{Re} \le 4000 \\ C = 0.193 & \text{m=0.618} & 4000 \le \mathrm{Re} \le 40000 \\ C = 0.027 & \text{m=0.805} & 40000 \le \mathrm{Re} \le 400000 \end{cases} \qquad (3.51)$$

where

Nu, Re, Pr are respectively the Nusselt, Reynolds and Prandtl numbers;

μ_f, k_f, c_f are the dynamic viscosity, thermal conductivity, specific heat of the working fluid evaluated at temperature T_f;

D_f and A_f are the external pipe diameter and the external tube surface in the condenser section;

C, m are fitting coefficients that allow to account for different flow regimes.

4 Numerical and parametric analysis

*T*his chapter provides a brief description of the numerical procedure used to solve the ODE system 3.43. The lumped parameter model has been updated including transfer limitations in order to consider a more realistic condition, and extended to different working fluids. Then the results of numerical simulations are presented in order to demonstrate that it is an optimal tool to execute parametric analysis useful in heat pipe design process.

4.1 Introduction

The numerical solution of the ODE system 3.43 representing the lumped parameter model has been implemented in C++ environment using GSL packages. The model is able to simulate the transient as well as the steady-state operation of a sintered heat pipe. It has been validated by comparisons with numerical and experimental results readily available from the open literature (C. Ferrandi [6]).

4.2 Numerical procedure

The main steps of numerical procedure are briefly described and represented in the algorithm flowchart of Figure 4.1.

Read inputs. Input values concerns

- heat pipe's geometry (L_{eva} , L_a , L_{cond} , d_{ep}, d_{ip}, d_{iw}),
- pipe's material (e.g., aluminum, copper, steel), chosen from a database listing material's properties (ρ, c, k),
- wick's type (e.g., sintered, packed sphere, wrapped screen),
- wick's properties (ε, r_g) ,
- working fluid (e.g. ammonia, ethanol, water),
- cooling fluid properties (T_f, h_f or $\dot{m}_f$),
- end time and time step.

Evaluate the convective coefficient. If the convective thermal coefficient of cooling medium is unknown, it is calculated from Nusselt number by means of the equation 3.51.

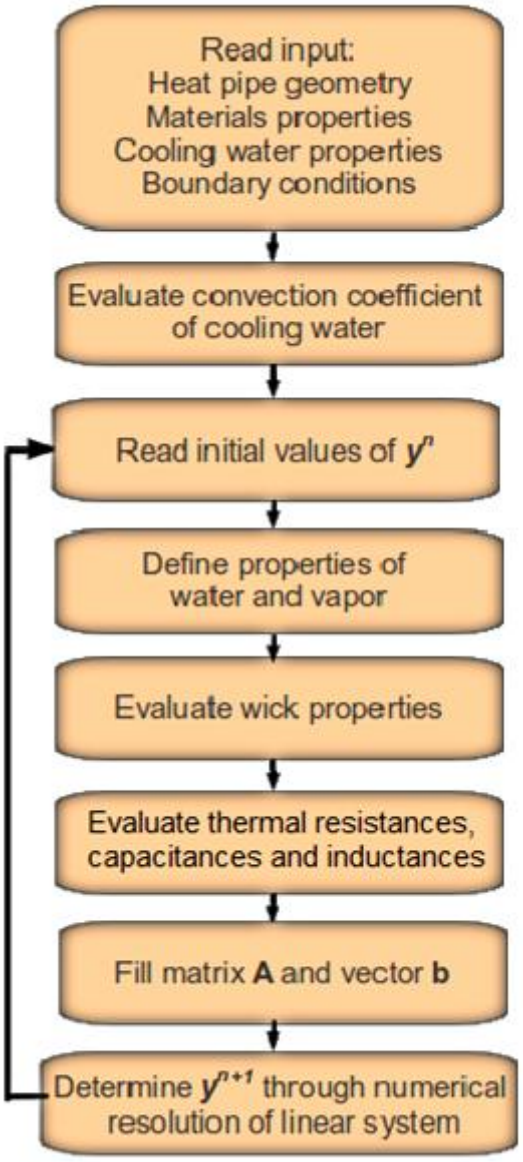

Figure 4.1 Flow chart of lumped parameter model

Read the initial conditions . At start time thermal equilibrium of heat pipe is assumed so the temperature of each node is set equal to initial value T_0. Mass flow rates are assumed to be equal to zero.

Define the properties of water and vapor. The working fluid properties $(\rho, c_p, p, \mu, k, \sigma, h_{lv})$, are calculated at nodal temperature by means of polynomial interpolation of the standard reference values given by NIST (E.W. Lemmon [16]).
Evaluate the wick's properties. A correction of the fluid properties (e.g., thermal conductivity k_l, thermal capacity C) is needed in order to consider the presence of liquid in the wick: a weighted average of the solid and liquid properties is implemented, as explained in paragraph 3.2.

Evaluate the resistances, capacitances, and inductances. It is then possible to evaluate thermal resistances and capacitances and fluidic resistances and inductances of lumped model.
Fill matrix $\underline{\boldsymbol{A}}$ and vector b. Applying a numerical integration method it is possible to define a system of linear equations.
The ODE system 3.43 is numerically integrated by means of a θ-method. Equation 3.45 is approximated with the following expression:

$$\boldsymbol{y}^{n+1} = \boldsymbol{y}^n + \Delta t\big((1-\theta)\boldsymbol{f}(t^{n+1}, \boldsymbol{y}^{n+1}) + \theta\, \boldsymbol{f}(t^n, \boldsymbol{y}^n)\big) \tag{4.1}$$

The parameter θ can be tuned obtaining different methods as listed in Table 4.1.

Table 4.1 Numerical integration methods

$\boldsymbol{\theta}$	Method	Formula
0	Backward Euler	$y^{n+1} = y^n + \Delta t\ f(t^{n+1}, y^{n+1})$
1	Forward Euler	$y^{n+1} = y^n + \Delta t\ \ f(t^n, y^n)$
0.5	Crank-Nicolson	$y^{n+1} = y^n + \Delta t\big(0.5\, f(t^{n+1}, y^{n+1}) + 0.5\ f(t^n, y^n)\big)$

Euler methods are first-order numerical scheme. Forward Euler method is one of the simplest method with slow convergence (~Δt) but it can be numerically unstable so particular attention should be put while setting the time step size. On the other hand backward Euler method is implicit, thus numerically stable but more costly in terms of computational time. Crank-Nicolson is a second-order method, implicit in time and unconditionally stable.
By applying the numerical scheme the equations are rewritten as a linear system:

$$\underline{\boldsymbol{A}}\,\boldsymbol{y} = \boldsymbol{b} \tag{4.2}$$

Linear system solution. The linear system can be solved using LU decomposition with partial pivoting. The square matrix $\underline{\boldsymbol{A}}$ has a LU decomposition into upper and lower triangular matrices

$$\underline{\boldsymbol{P}}\,\underline{\boldsymbol{A}} = \underline{\boldsymbol{L}}\,\underline{\boldsymbol{U}} \tag{4.3}$$

where $\underline{\boldsymbol{P}}$ is a permutation matrix, $\underline{\boldsymbol{L}}$ is a unit lower triangular matrix and $\underline{\boldsymbol{U}}$ is a upper triangular matrix. The linear system of eq. 4.2 is converted into a pair of triangular linear systems

$$\begin{cases} \underline{\boldsymbol{L}}\boldsymbol{x} = \underline{\boldsymbol{P}}\mathbf{b} \\ \underline{\boldsymbol{U}}\boldsymbol{y} = \boldsymbol{x} \end{cases} \tag{4.4}$$

which can be solved by forward- and back-substitution, obtaining temperatures, pressures and mass flow rates at various locations in the heat pipe.
The procedure repeats for each time step.

4.3 Heat pipe performances

Once temperature are obtained other parameters such as heat fluxes, temperature gradients, heat pipe efficiency can be easily calculated.
The heat pipe's effective thermal resistance is the overall resistance between evaporator and condenser and it is defined as follows

$$R_{\mathrm{HP}} = \frac{T_{\mathrm{eva}} - T_{\mathrm{cond}}}{\dot{Q}_{\mathrm{IN}}} \tag{4.5}$$

For a constant temperature jump between evaporator and condenser regions, the lower is the resistance R_{HP} the higher is the transmitted heat power $\dot{Q}_{\mathrm{IN}}$.
It is also important to check the level of evaporator dryness χ represented by the percentage ratio between the liquid mass in the evaporator wick M_e and the liquid mass that could fill the same volume of wick at the same temperature M_{e0}.

$$\chi = 100\,\frac{M_e}{M_{e0}} \tag{4.6}$$

Transport limitations are also considered evaluating heat power in the evaporator with the following expression,

$$Q_v = \frac{T_{we} - T_{ve}}{R_{2we}} \tag{4.7}$$

and comparing it with the maximum thermal power available from literature and listed in Table 4.1.

Table 4.1 Maximum thermal powers in heat pipe transport limitations (J. Ochterback [17])

Transfer limitations	Maximum thermal power [W]
Boiling limit	$\dot{Q}_{\text{boiling}} = \frac{2\pi L_{\text{eff}} k_{\text{eff}} T_{ve}}{A_v h_{lv} \rho_{ve} \ln\left(\frac{r_{int}}{r_{iw}}\right)} \left[\frac{2\sigma}{r_n} - \frac{2\sigma}{r_c}\right]$
Capillary limit	$\dot{Q}_{capillary} = \frac{\frac{2\sigma}{r_c}}{(F_l + F_v) L_{\text{eff}}}$ $\begin{cases} F_v = \frac{(f_v \text{Re}_v)\mu_{ve}}{2 r_{iw}^2 A_v \rho_{ve} h_{lv}} \\ F_l = \frac{\mu_{le}}{K A_w \rho_{le} h_{lv}} \end{cases}$
Entrainment limit	$\dot{Q}_{\text{entrainment}} = A_v h_{lv} \sqrt{\frac{\sigma \rho_{ve}}{2 r_c}}$
Viscous limit	$\dot{Q}_{\text{viscous}} = \frac{A_v r_{iw}^2 h_{lv} \rho_{ve} p_{ve}}{16 \mu_{ve} L_{\text{eff}}}$
Sonic limit	$\dot{Q}_{\text{sonic}} = A_v h_{lv} \sqrt{\frac{\gamma \rho_o p_0}{2(\gamma + 1)}}$

4.4 Parametric analysis

The aim of the numerical investigation presented in this paragraph is to estimate heat pipe performances for different working fluids and input power levels at evaporator section. A parametric analysis on the evaporator length is provided too.
Results obtained with fluids with similar operative temperature ranges, such as water and ethanol, have been compared.

Three different materials have been chosen for the heat pipe tube and wick domains: aluminum, copper and stainless steel.
Materials' properties are listed in Table 4.2

Table 4.2 Materials' properties

	Aluminum	Copper	Stainless steel
ρ [kg/m³]	2700	8920	7950
k [W/m K]	230	390	43
c [J/kg K]	900	380	480

4.4.1 Ethanol-copper and water-copper sintered heat pipe

Simulations for a copper sintered heat pipe with ethanol or water as working fluid have been performed with the input values listed in Table 4.3.

Table 4.3 Inputs for lumped parameter analysis of ethanol-copper and water-copper heat pipes

Geometry			
d_{ep} [mm]	6	L_{eva} [mm]	80
d_{ip} [mm]	5	L_a [mm]	50
d_{iw} [mm]	3	L_{cond} [mm]	60
Wick's properties		**Initial temperature and cooling fluid properties**	
ε	0.7	T_0 [°C]	20
r_g [µm]	50	T_f [°C]	10
		h_f [W/m²K]	400

Figure 4.2 shows the heat pipe transient response (heat power released by the condenser to the cold sink) to a step function heat-up of 5 W for water and ethanol.
At start time convective power is different from zero because of the jump of temperature between initial temperature of condenser section and cooling fluid temperature. For equal operative conditions and the same heat pipe's structure water-copper heat pipe releases a greater amount of heat power to the cold sink than ethanol-copper heat pipe.

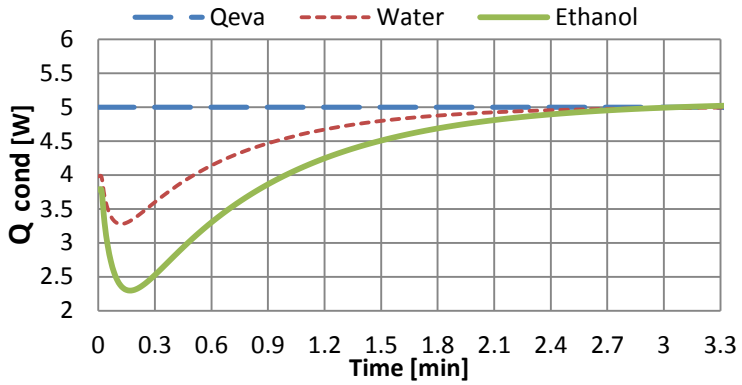

Figure 4.2 Convective power for water and ethanol heat pipe for a step function heat-up of 5W (L_{eva}=80mm)

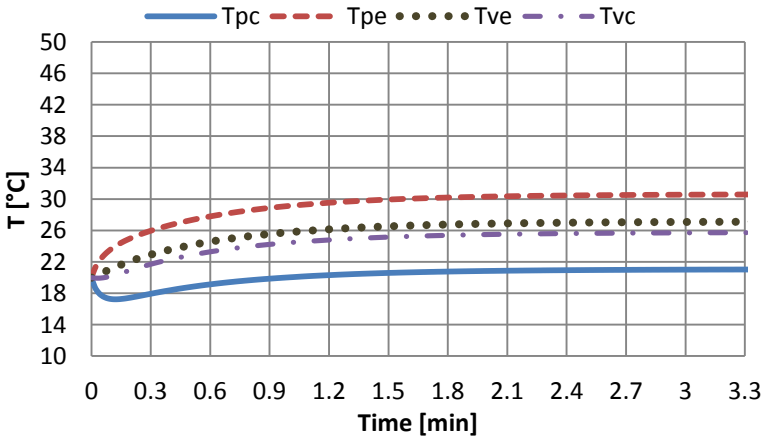

Figure 4.3 Water-copper heat pipe. Wall and vapor temperatures for step function heat-up of 5W (L_{eva}=80mm)

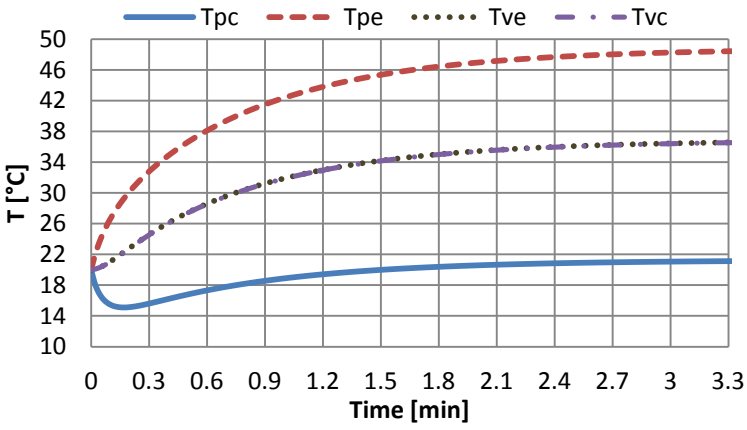

Figure 4.4 Ethanol-copper heat pipe. Wall and vapor temperatures for step function heat-up of 5W (L_{eva}=80mm)

Figure 4.3 and Figure 4.4 illustrate the trends of wall and vapor temperatures of the water-copper and ethanol-copper heat pipes. The temperature jump between evaporator and condenser sections is higher for ethanol-copper heat pipe ($\sim 26\,K$) than water-copper heat pipe ($\sim 8\,K$), thereafter a water-copper heat pipe is more efficient in such operative conditions and for the heat pipe features listed in Table 4.3.
Since one of the purposes of the analysis is to find out the influence of evaporator length on the heat pipe's performances, evaporator length has been changed keeping constant the overall length of pipe and the dimension of condenser as shown in Table 4.4.

Table 4.4 Input for parametric analysis on evaporator length

Length of heat pipe sections	SIM 1	SIM 2	SIM 3
L_{eva} [mm]	**80**	**60**	**40**
L_a [mm]	**50**	**70**	**90**
L_{cond} [mm]	60	60	60
Total length [mm]	190	190	190

In Figure 4.5 and Figure 4.6 the mid-wall temperature of evaporator section is plotted for different evaporator lengths and working fluids. Decreasing evaporator length the temperature increases degrading heat pipe performances. The effects of reduced evaporator dimensions are more appreciable for ethanol- copper heat pipe.

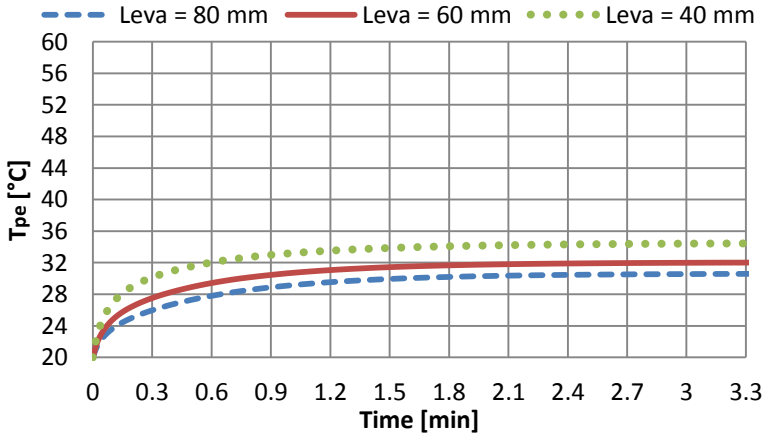

Figure 4.5 Water-copper heat pipe. Temperature of evaporator wall with a step function heat-up of 5W

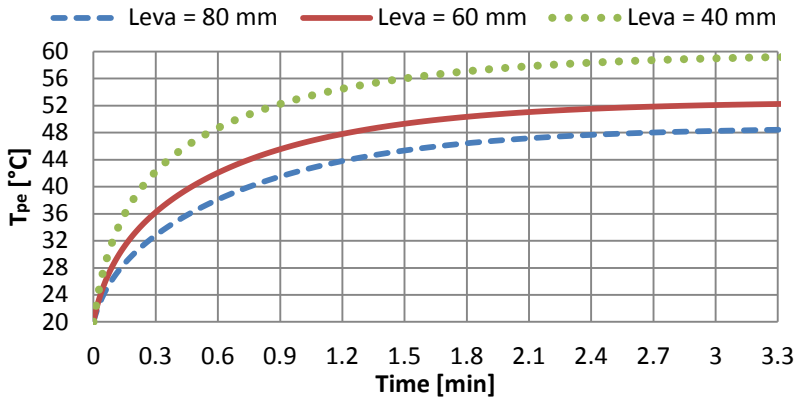

Figure 4.6 Ethanol-copper heat pipe. Temperature of evaporator wall with a step function heat-up of 5W

In order to investigate transfer limitations of heat pipe a step function heat-up is applied to evaporator section increasing power of 5 W every 200 seconds. The results of the analysis presented hereafter refer to a water-copper heat pipe.

Figure 4.7 shows the incoming heat power of evaporator section.

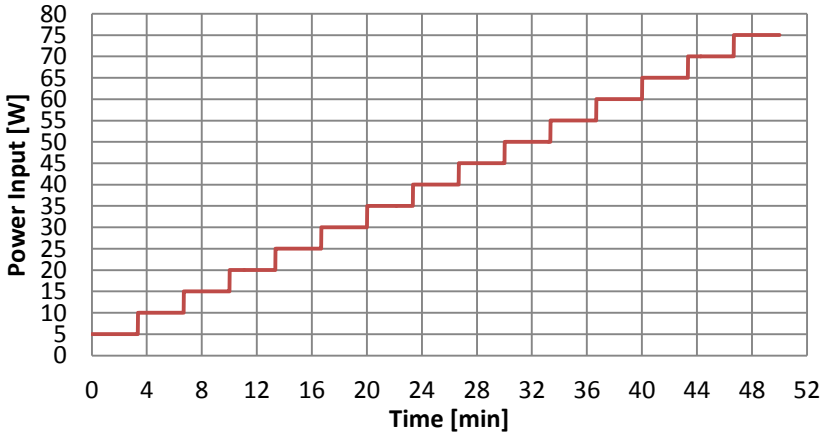

Figure 4.7 Water-copper heat pipe. Step function heat-up

The results of the analysis are shown in Figure 4.8 in terms of wall temperatures of evaporator and condenser sections and vapor temperature. For each step of heat-up the temperatures achieve a steady-state condition. A 60W power input is sufficient to cause nucleate boiling in the evaporator wick reducing heat pipe performances.

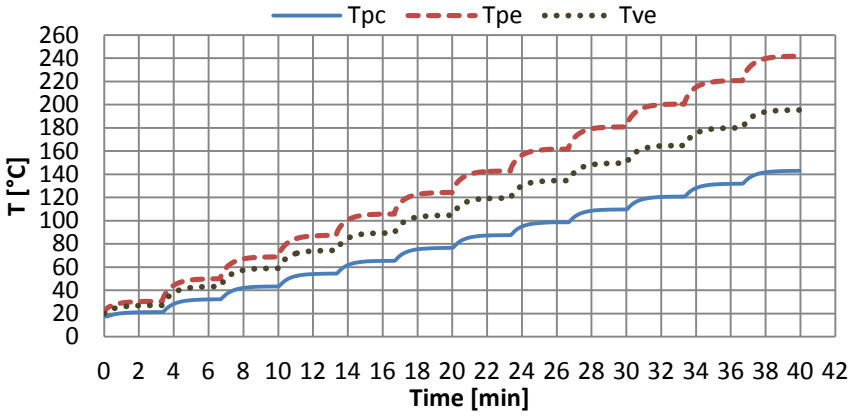

Figure 4.8 Water-copper heat pipe. Wall temperatures for evaporator and condenser sections and vapor temperature (L_{eva}=80mm)

A parametric analysis on the effects of the evaporator length on transfer limitations of heat pipe is also provided. For the evaporator lengths considered for the analysis 60W power is the maximum heat power input for boiling limit. Decreasing the evaporator length the phenomenon tends to anticipate, however the differences in terms of time are negligible (see Figure 4.9).

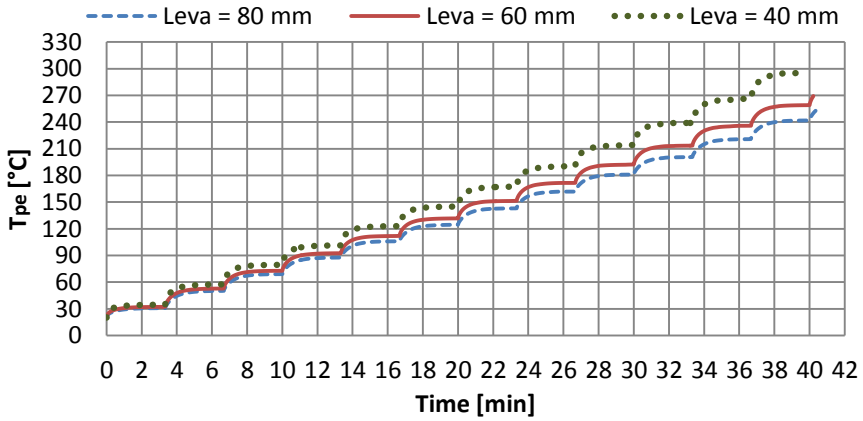

Figure 4.9 Water-copper heat pipe. Temperature of evaporator wall for different evaporator lengths

The heat pipe performances are also estimated in terms of overall resistance defined by eq. 4.5. Increasing the input power level the heat pipe resistance decreases, however when the power level is closed to maximum power limit the heat pipe resistance increases because of performance losses caused by transfer limitations, as shown in Figure 4.10. Furthermore heat pipe resistance is significantly influenced by

evaporator length. For a fixed value of power input and reducing evaporator's dimensions the resistance increases because of the higher value of evaporator temperature (see Figure 4.9).

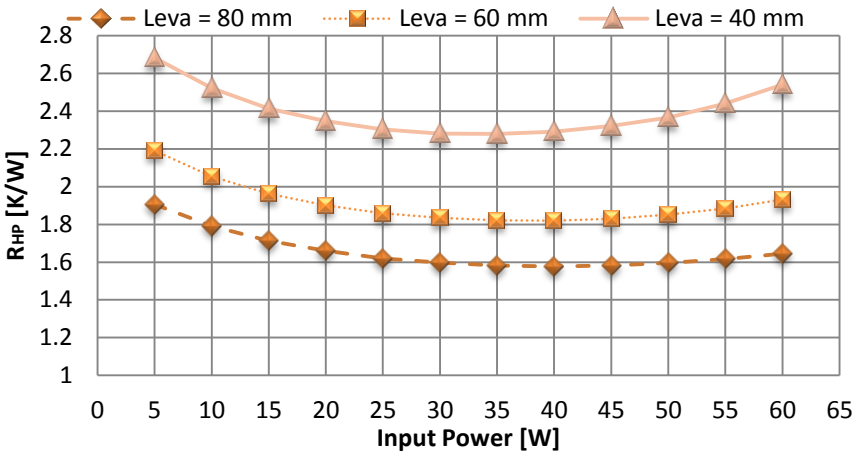

Figure 4.10 Water-copper heat pipe. Overall resistance

The level of evaporator dryness is also estimated for the water-copper heat pipe at steady-state conditions. The level of dryness decreases for higher values of power inputs and more rapidly if the evaporator section is shortened as illustrated in Figure 4.11.

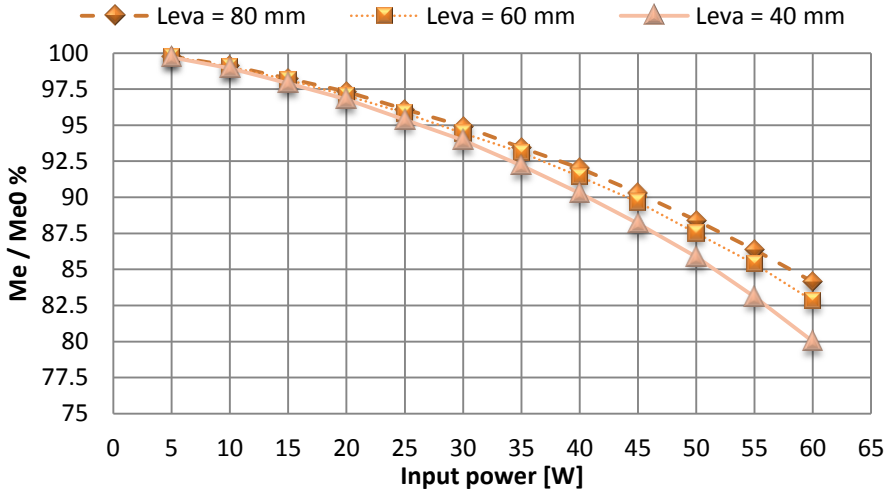

Figure 4.11 Water-copper heat pipe. Level of evaporator dryness

5 Heat pipe hybrid analysis: coupling of lumped and distributed parameter models

*T*his chapter represents the core of this research study. It focuses on the interaction between the finite volume and lumped parameter models and stresses the main issues concerning numerical coupling of the two models. Coupling is based on the integration of the heat pipe lumped model (developed in C++ language) with the finite volume solver OpenFOAM. First a brief overview of OpenFOAM potential is presented. Eventually the main results obtained by the hybrid solver are illustrated and compared with the simulations based on a finite element analysis.

5.1 Introduction

Lumped parameter simulation of heat pipe offers excellent results concerning heat pipe behavior, and it is an optimal design tool. Nevertheless in many applications heat pipes are embedded or coupled to external solid components (i.e. the heat generating component which needs to be cooled), thus boundary condition at evaporator section is not well-known. In these applications simple geometries can be reduced to a lumped parameter model expanding heat pipe's model, while for complex geometries lumping approach could result too rough or even inapplicable, thereafter a distributed approach analysis (i.e. finite volumes or finite elements analysis) is preferable for the external domain. Here two approaches are likely possible, that is running finite volume analysis of solid and lumped analysis of heat pipe sequentially or in parallel.

Serial approach

The serial approach consists in running the two codes separately : the external solid wall conduction problem is solved by the Finite Volume Model (FVM), thereafter the lumped parameter model of the heat pipe is

run. In particular the presence of the heat pipe in the FVM is modeled as an overall convective boundary condition at the surface in contact with the heat pipe evaporator wall. The FVM simulation output is the heat power input to the heat pipe. Indeed this value is used as boundary condition in the lumped parameter model which will provide the new heat pipe overall convective thermal coefficient. Actually it is necessary to choose an initial guess of the heat pipe overall convective coefficient, run the two simulations and repeat until convergence of heat power values. This approach results too hardworking and computationally expensive.

Parallel approach

The parallel approach consists in running the two codes in parallel . The FVM interacts with lumped parameter model of heat pipe at each time step by means of the boundary condition. This approach is clearly more efficient, and more accurate in transient analysis. To put into practice this procedure it is necessary a customizable finite volume solver in order to modify solving equations at will and allow a real-time interaction of the two models creating a hybrid solver. OpenFOAM is one of the finite volume solvers that meets this criteria.

5.2 Introduction to OpenFOAM

OpenFOAM® (Open Field Operation and Manipulation) is a C++ toolbox for the development of customized numerical solvers for the solution of continuum mechanics problems, including computational fluid dynamics (CFD). The code, produced by OpenCFD Ltd., is released as free and open source software under the GNU General Public License and it is currently distributed for Linux operating systems. It has a large user base across most areas of engineering and science and an extensive range of features to solve different kinds of problems from complex fluid flows involving chemical reactions, turbulence and heat transfer, to solid dynamics and electromagnetics. It also includes tools for meshing and for pre- and post-processing, running in parallel.

*"OpenFOAM is first and foremost a C++ library, used primarily to create executables, known as applications. The applications fall into two categories: **solvers**, that are each designed to solve a specific problem in continuum mechanics; and **utilities**, that are designed to perform tasks that involve data manipulation."* (OpenFoam [18])

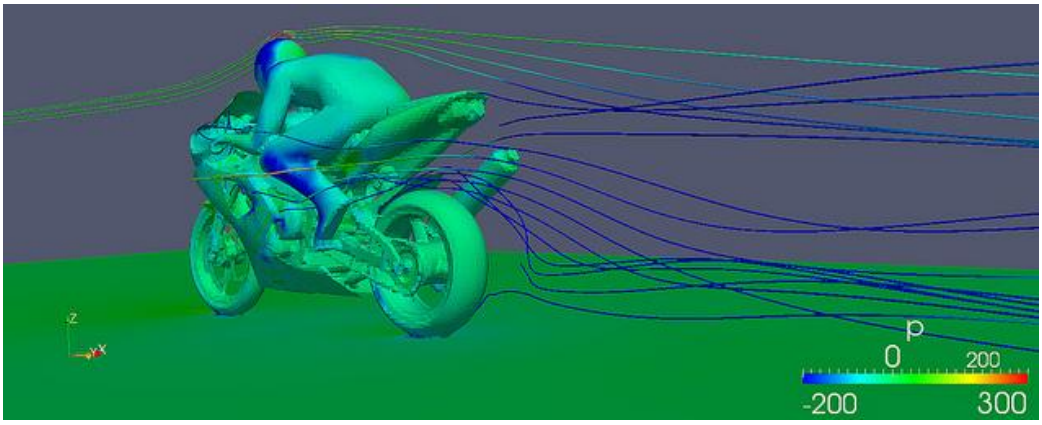

Figure 5.1 Example of OpenFOAM simulation: streamlines and pressure distribution on a motorbike

The main advantages of this software are the options to customize existing solvers or to create new ones, the friendly syntax for partial differential equations and the freeware license. Thence it is possible to incorporate the lumped parameter code in a OpenFOAM solver in order to run the lumped parameter analysis and the FVM's simulation in parallel.

5.3 OpenFOAM structure

The solution of a problem (or case) in OpenFOAM environment requires a well-defined directory structure and files organization. The basic directory structure for an OpenFOAM case is shown in Figure 5.1.

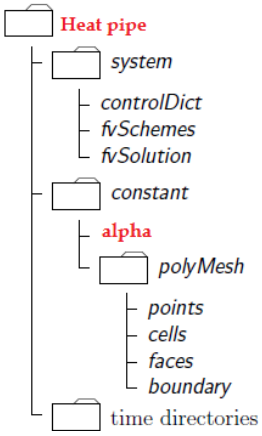

Figure 5.1 Case directory structure

The main folder, named **HeatPipe**, contains three subfolders:

- A **system** directory for setting parameters associated with the solution procedure itself. It contains at least the following files:
  - **controlDict** where run control parameters are set including start/end time, time step and parameters for data output;
  - **fvSchemes** where discretization schemes may be selected at run-time;
  - **fvSolution** where the equation solvers, tolerances and other algorithm controls are set.
- A **constant** directory containing a full description of the case mesh in a subdirectory **polyMesh** and files specifying physical properties for the application concerned, e.g. alpha.

The **time directories** contain individual files of data for particular fields, e.g. temperature, temperature gradient. The data can be either user-defined initial values and boundary conditions or results written to file by the OpenFOAM solver. The name of each time directory is based on the simulated time at which the data is written. Since simulations start usually at time t=0, the initial conditions are stored in a directory named 0. The OpenFOAM fields must always be initialized, even when the solution does not strictly require it, as in steady-state problems.

5.3.1 Numerical schemes and solution algorithm

The following numerical schemes have been specified for first time derivative, gradient and laplacian operators.

```
ddtSchemes
{
    default         Euler implicit;
}
gradSchemes
{
    grad(T)         Gauss linear;
}
laplacianSchemes
{
    laplacian(DT,T) Gauss linear corrected;
}
```

Additionally a linear scheme is selected for point-to-point interpolations of values from cells centers to face centers, and flux generation for temperature field is also required.

```
interpolationSchemes
{
    default         linear;
}
fluxRequired
{
    T;
}
```

5.3.2 Mesh generation

Mesh is described in the **polyMesh** sub-folder. It contains files with lists of points, faces and cells composing the mesh. Boundary faces coinciding with the domain boundary are divided from the internal faces and they are listed in group of faces constituting a boundary surface, called patch. The solid domain boundary is generally broken up into a set of patches. One patch may include one or more enclosed areas of the boundary surface which do not necessarily need to be physically connected. **Boundary** file contains a list of patches each of which is associated with a boundary condition:

```
ADIABATIC_SURFACE
{
    type            patch;
    nFaces          1262;
    startFace       159516;
}
OUTER_SURFACE
{
    type            patch;
    nFaces          400;
    startFace       160778;
}
INNER_SURFACE
{
    type            patch;
    nFaces          578;
    startFace       163018;
}
```

OpenFOAM provides different utilities for the creation of meshes, e.g. **blockMesh** utility for generating simple meshes of blocks of hexahedral cells or **snappyHexMesh** utility for generating complex meshes of hexahedral and split-hexahedral cells automatically from triangulated surface geometries. By default OpenFOAM defines a mesh of arbitrary polyhedral cells in 3D, bounded by arbitrary polygonal faces, i.e. the cells can have an unlimited number of faces where, for each face, there is

no limit on the number of edges nor any restriction on its alignment. This type of mesh generation and manipulation is more suitable for complex geometries.
Since OpenFOAM has no graphic tool to generate geometry and mesh, it could be more convenient, specially for complex geometries, to generate mesh with a CAD software and then import the mesh into OpenFOAM environment. For this purpose different options are available for conversion of a mesh into OpenFOAM format.

5.3.3 Boundary conditions

Since a patch contains no geometric or topological information about the mesh, in **boundary** file it is necessary to specify the type of boundary condition. The patch types typically used in heat transfer analysis are listed in Table 5.1.

Table 5.1 Patch types associated with different boundary conditions

Patch type	Boundary condition
fixedValue	Imposed temperature
fixedGradient	Imposed flux
zeroGradient	Adiabatic

It is relevant to specify that for Neumann boundary condition the heat flux is imposed in terms of temperature gradient, easily obtained from the following expression:

$$\dot{Q} = -kA\,\frac{\partial T}{\partial r} \tag{5.1}$$

5.3.4 Initial conditions

To solve a problem initial condition must be assigned for the internal and boundary fields using the following syntax:

```
internalField              uniform 290.;

boundaryField
{
    ADIABATIC_SURFACE
    {
        type              zeroGradient;
    }
```

```
    OUTER_SURFACE
    {
        type            fixedValue;
        value           uniform 350.;
    }
    EVAPORATOR
    {
        type            fixedGradient;
        gradient        uniform -1000.;
    }
}
```

5.4 Hybrid solver design

In order to check out the coupling of the heat pipe lumped model and the external solid FVM where the heat pipe is embedded, it is necessary to build a CAD model of the solid. The finite volume model is composed by a cylinder shaped tube that envelops the heat pipe evaporator section (Figure 5.2).

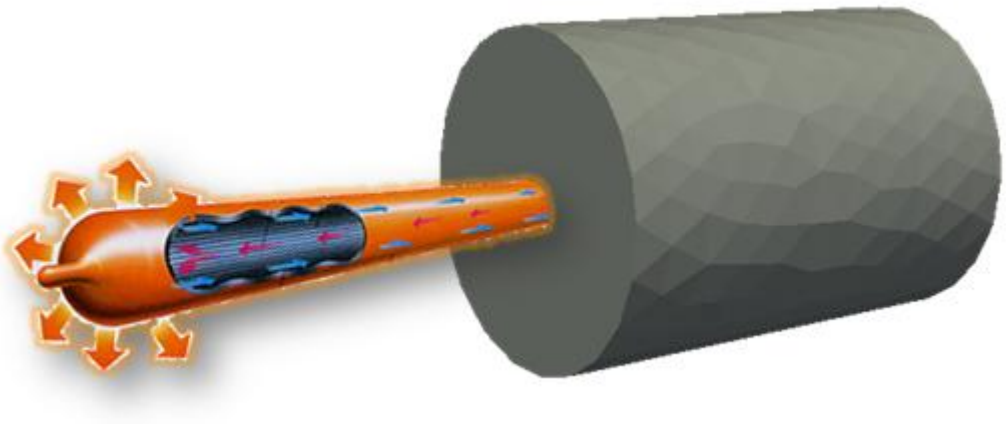

Figure 5.2 Heat pipe embedded in solid volume

Even if the geometry is quite simple, an external software with graphic interface like SALOME has been preferred to OpenFOAM to create the geometry and build the mesh. SALOME is an open-source software that provides a generic platform for pre- and post-processing for numerical simulations.
To convert to OpenFOAM format the mesh generated by Salome and exported as UNV file it is sufficient to use the command

"ideasUnvToFoam". Once the mesh is imported it is convenient to check mesh, that must satisfy a fairly stringent set of validity constraints to ensure a valid and accurate solution. Figure 5.3 shows the solid domain mesh. A mesh refinement on the inner surface is required in order to obtain a better spatial discretization and a more accurate solution. Mesh size becomes coarser for increasing curvature radii resulting in a loss of accuracy but also in less computational time.

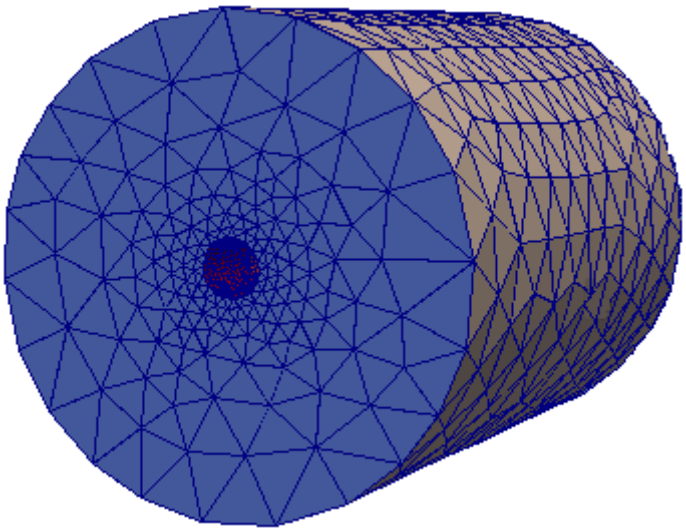

Figure 5.3 Solid domain mesh

Figure 5.4 shows a wireframe view of mesh in order to highlight the channel where the heat pipe is inserted.

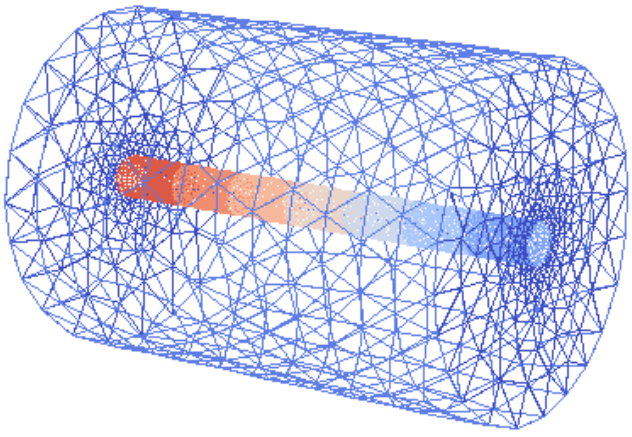

Figure 5.4 Solid domain mesh – Wireframe view

Lumped and distributed parameter models are coupled by means of boundary conditions.

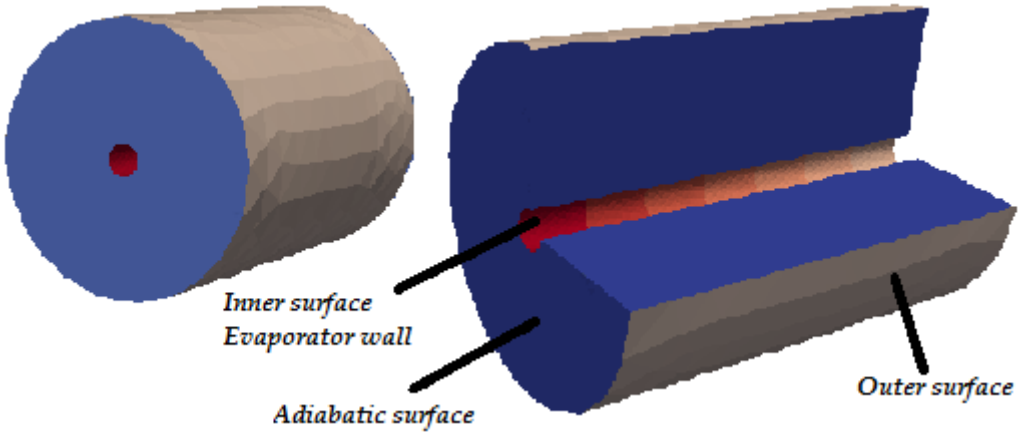

Figure 5.5 Sketch of solid domain and boundary surfaces

Given the boundary condition on the outer surface of solid domain (see Figure 5.5) the transient heat equation is solved:

$$\frac{\partial T}{\partial t} = \frac{1}{\alpha}\nabla^2 T \tag{5.2}$$

where α is the thermal diffusivity of material defined as follows

$$\alpha = \frac{k}{\rho c} \tag{5.3}$$

Taking advantage of one distinguishing feature of OpenFOAM, that is its syntax for tensor operations and partial differential equations that closely resembles the equations being solved, eq. 5.2 can be easily implemented in a OpenFOAM solver as follows:

```
solve
(
    fvm::ddt(T) - fvm::laplacian(alpha, T)
);
```

Once the temperature field distribution on the inner surface of solid is determined it is possible to set the boundary condition on evaporator surface of the heat pipe, that is an input value for the lumped parameter model. Then the solution of lumped parameter model allows to update the boundary condition of finite volume model.
The conceptual scheme of hybrid solver is illustrated in Figure 5.6.

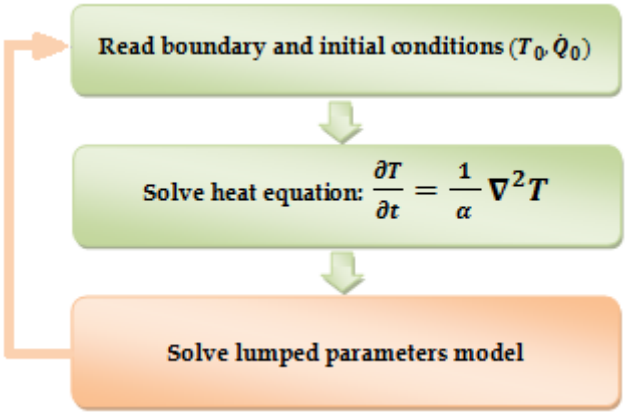

Figure 5.6 Conceptual scheme of hybrid solver

Hybrid solver couples lumped and distributed parameter models by means of boundary conditions, as already explained. Once the temperature field on the inner surface of cylinder is determined, an average value of faces temperatures is calculated.

$$T_{\text{mean}} = \frac{\sum_{i=1}^{Nfaces} Ti}{N_{faces}} \tag{5.4}$$

This is considered a good approximation since the faces have a regular shape as shown in Figure 5.7, otherwise the average integral of temperature is more suitable:

$$T_{\text{mean}} = \frac{\iint T dS}{S} \tag{5.5}$$

where S is the inner surface of tube.

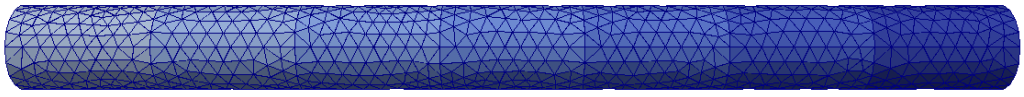

Figure 5.7 Mesh of inner surface of solid domain

The average value of the temperature corresponds to the outer surface of evaporator section T_{eva}, which represents an input value of lumped parameter model.

$$T_{\text{eva}} = T_{\text{mean}} \tag{5.6}$$

The structure of hybrid solver is represented in the algorithm flowchart of Figure 5.9. The main steps of numerical procedure are briefly described as follows:

1) **Read the boundary and initial conditions and time t^n.** Read thermal boundary conditions on solid domain boundary surfaces and initial temperature of internal domain.

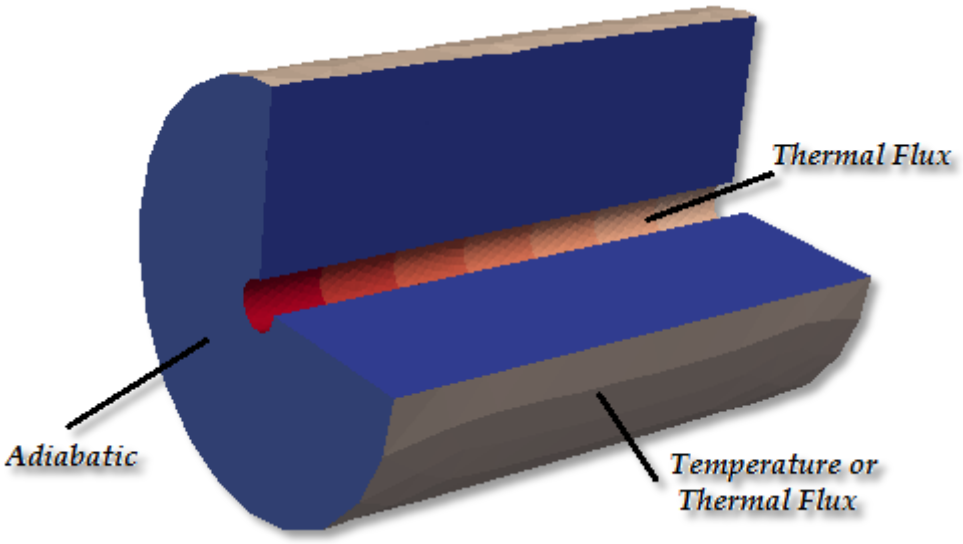

Figure 5.8 Solid domain boundary conditions

2) **Solve the heat equation** to define temperature field of solid domain at time t^{n+1}.
3) **Evaluate the average temperature of inner surface $\tilde{T}_{\text{eva}}^{n+1}$.** The average temperature, calculated as in eq. 5.4, represents the evaporator outer wall temperature $\tilde{T}_{\text{eva}}^{n+1}$ of heat pipe as stated in eq. 5.6.
4) **First guess of evaporator input power.** Once the evaporator outer wall temperature is calculated, it is possible to evaluate the input of lumped parameter model, that is the evaporator power input $\dot{\tilde{Q}}_{IN}^{n+1}$ referring to eq. 3.47 and Figure 3.1. Since the evaporator mid-wall temperature T_{pe} at time t^{n+1} is unknown, $\dot{\tilde{Q}}_{IN}^{n+1}$ is estimated as follows

$$\dot{\tilde{Q}}_{IN}^{n+1} = -\frac{T_{pe}^{n} - \tilde{T}_{\text{eva}}^{\text{n+1}}}{R_{1pe}} \qquad (5.7)$$

and represents a first guess input of lumped parameter model.

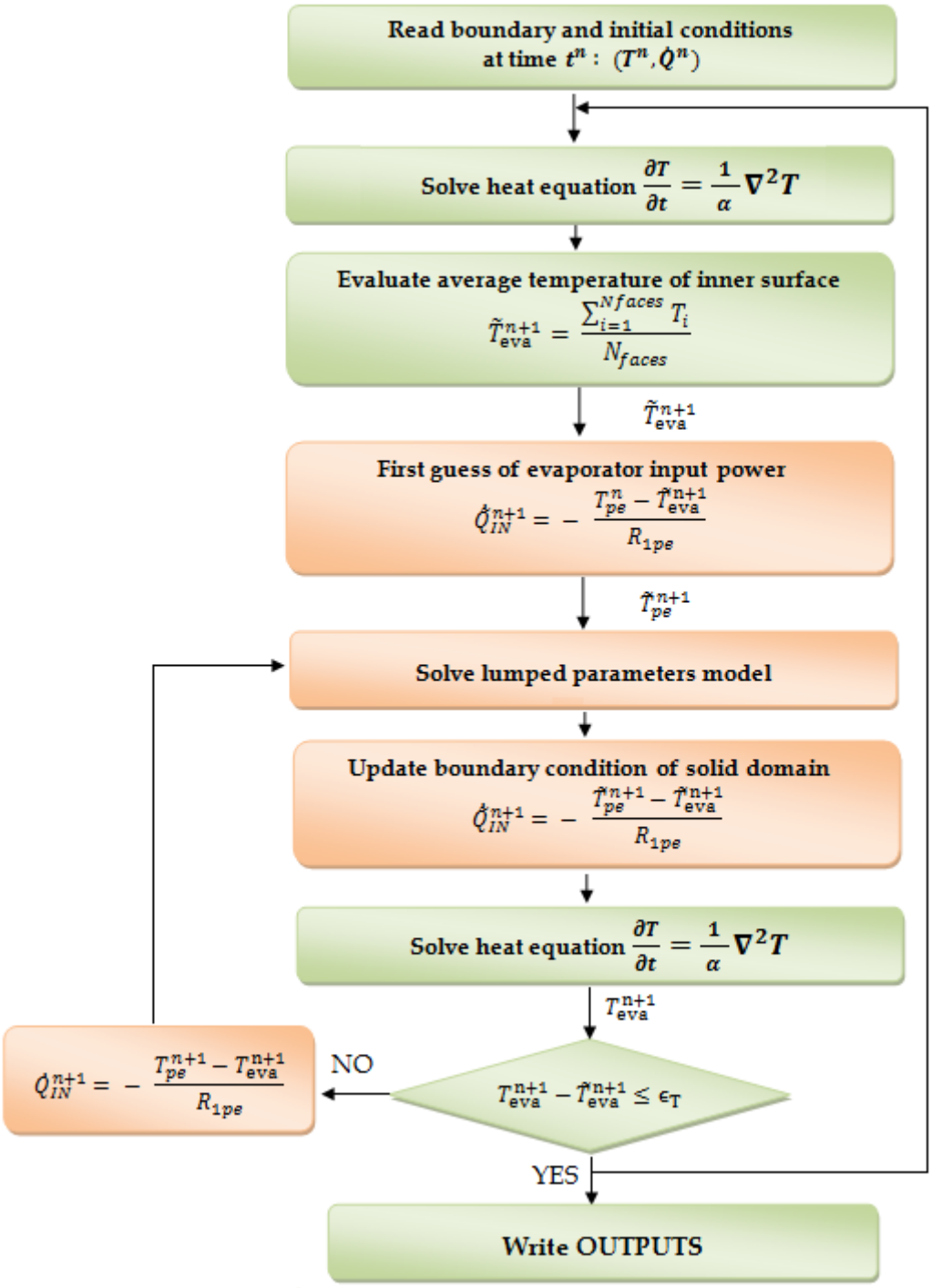

Figure 5.9 Flowchart of hybrid solver
red blocks: lumped parameter model
green blocks: finite volumes model

5) **Solve the lumped parameter model.** Lumped parameter model is solved so the evaporator mid-wall temperature T_{pe} is updated at time t^{n+1}.
6) **Update the boundary condition of the solid domain.** The evaporator power input $\dot{\tilde{Q}}_{IN}^{n+1}$ is updated as follows

$$\dot{\tilde{Q}}_{IN}^{n+1} = -\frac{\tilde{T}_{pe}^{n+1} - \tilde{T}_{\mathrm{eva}}^{\mathrm{n+1}}}{R_{1pe}} \tag{5.8}$$

and it represents the new inner surface boundary condition of finite volume model.
7) **Solve the heat equation.** The temperature field of solid domain is updated and the average temperature of inner surface $T_{\mathrm{eva}}^{\mathrm{n+1}}$ is evaluated.
8) **Check of evaporator outer wall temperature.** If the following expression is satisfied,

$$T_{\mathrm{eva}}^{\mathrm{n+1}} - \tilde{T}_{\mathrm{eva}}^{\mathrm{n+1}} \leq \epsilon_{\mathrm{T}} \tag{5.9}$$

that is the error between the updated value of evaporator temperature $T_{\mathrm{eva}}^{\mathrm{n+1}}$ and the approximation $\tilde{T}_{\mathrm{eva}}^{n+1}$ is less than a tolerance value ϵ_{T} (i.e. 10^{-4}), the solution is accepted, otherwise evaporator power input is updated as follows

$$\dot{Q}_{IN}^{n+1} = -\frac{T_{pe}^{n+1} - T_{\mathrm{eva}}^{\mathrm{n+1}}}{R_{1pe}} \tag{5.10}$$

the lumped parameter model is solved again and procedure is repeated from step 5) until the expression of eq. 5.9 is satisfied.
9) **Write OUTPUTS.** Results at time t^{n+1} are written to files and they represent the boundary and initial conditions for next time step. Time is advanced in step and simulation continues from step 1) in order to determine the solution at time t^{n+2}.

5.4.1 Numerical approach to coupling issue

The approach presented in paragraph 5.4 is based on a fixed-point iteration in order to determine the boundary condition at the heat pipe-solid domain interface. An iterative procedure is needed to avoid the temporal mismatch of solutions obtained with lumped and distributed

parameter models, since the boundary heat power is approximated with the temperatures evaluated in different time steps (see eq. 5.7).
Since in solid domain the output power of inner surface causes a decrease of local temperature on boundary faces, the following condition could occur:

$$T_{\text{eva}}^{\text{n+1}} < T_{\text{eva}}^{\text{n}} \tag{5.11}$$

Since the heat pipe wall thickness is very small (≈ 1mm), the mid-wall temperature T_{pe}^{n} and the evaporator outer surface temperature $T_{\text{eva}}^{\text{n}}$ are very similar. If the condition expressed by eq. 5.11 occurs, the following expression could also be satisfied:

$$T_{\text{eva}}^{\text{n+1}} < T_{pe}^{n+1} \tag{5.12}$$

Referring to eq. 5.10, in such condition the power input changes sign so boundary condition of output power for solid domain is converted in a input power condition. Thereafter the temperature of the solid domain inner surface increases and starts oscillating (see Figure 5.10).

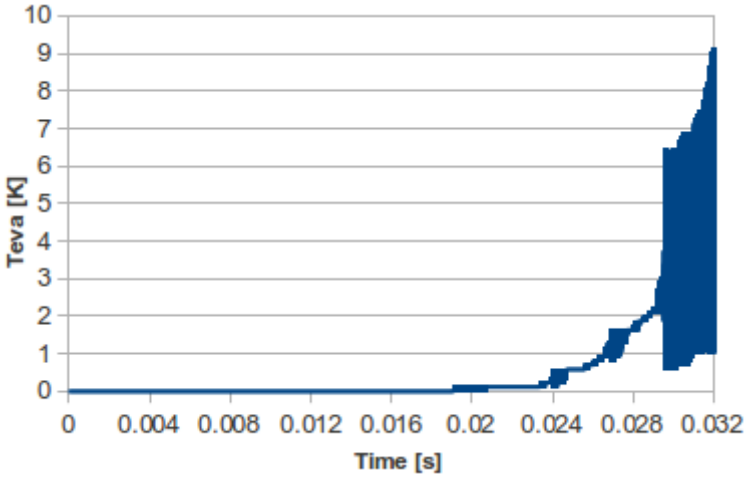

Figure 5.10 Oscillation of evaporator temperature

The oscillation of boundary condition causes numerical instability since the error grows exponentially and solution does not converge, as shown in Figure 5.11.

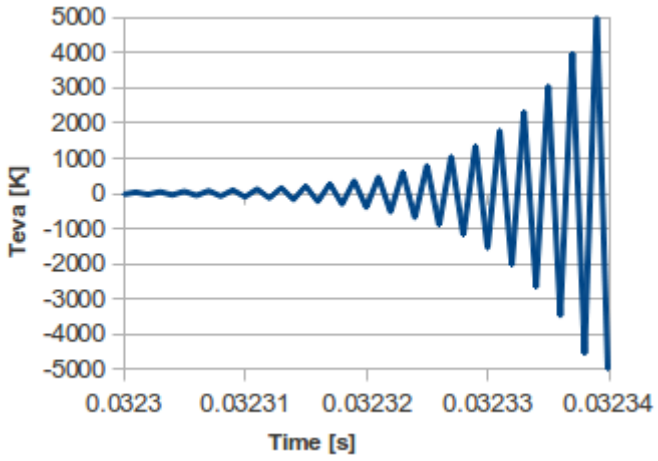

Figure 5.11 Oscillation of evaporator temperature and numerical instability

So as to improve numerical stability different techniques have been considered and some of the successful attempts are here reported.
The first effort to overcome the numerical instability is based on a c**onditioning solution,** that is to constrain the solution of temperature field to follow a certain trend according to the sign of heat power of boundary condition. It has been observed that when the temperature decreases, the absolute value of heat power tend to decrease too until it changes sign. Therefore the following correction has been introduced:

$$if\ \left(sign\left(\dot{Q}_{IN}^{n+1}\right) \neq sign(T_{\mathrm{eva}}^{\mathrm{n+1}} - T_{\mathrm{eva}}^{\mathrm{n}})\right) \qquad T_{\mathrm{eva}}^{\mathrm{n+1}} = T_{\mathrm{eva}}^{\mathrm{n}} \tag{5.13}$$

At each iteration the signs of heat power and the first time derivative of temperature on boundary surface are compared; if they are not equal the value of temperature $T_{\mathrm{eva}}^{\mathrm{n+1}}$ is considered physically inacceptable and it is overwritten with temperature at preceding time step. One of the main concerns was the delay introduced in numerical propagation. In this regard the percentage of corrections, that is the number of times that the value of temperature T_{eva} is overwritten, is evaluated and it is plotted as function of time steps in graph of Figure 5.12 (i.e. for a simulation time step equal to 0.001 the corrections occur 45% of time steps). Supposing that each correction induces a propagation delay of numerical solution equal to time step, the overall propagation delay is estimated as follows:

$$\frac{Nr.of\ corrections}{Nr.of\ time\ steps}\Delta t$$

Figure 5.13 shows the delay of numerical propagation as function of time steps. The estimated time delay is one order of magnitude less than time step so it is considered negligible, and it has no remarkable effects on the dynamic of heat pipe.

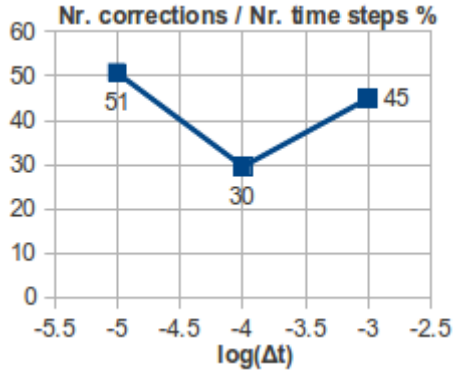

Figure 5.12 Percentage of number of corrections in function of time steps

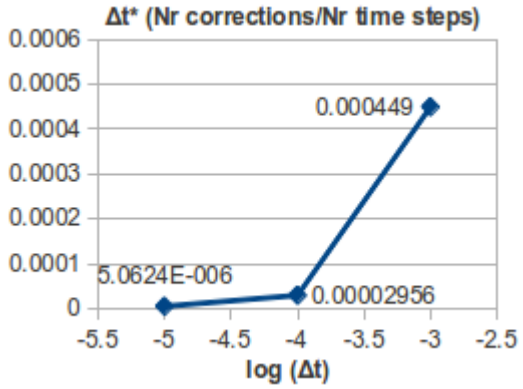

Figure 5.13 Delay of numerical propagation as function of time steps

The approach based on a conditioning solution provides good results, however it is not completely reliable since it is sensible to time stepping and might induce numerical errors that cause erroneous drift of solution. Reducing the time step the temperature curves graph tend to overlap, but approaching steady-state condition the solution drifts achieving a steady-state temperature less than the expected value, as shown in Figure 5.14.

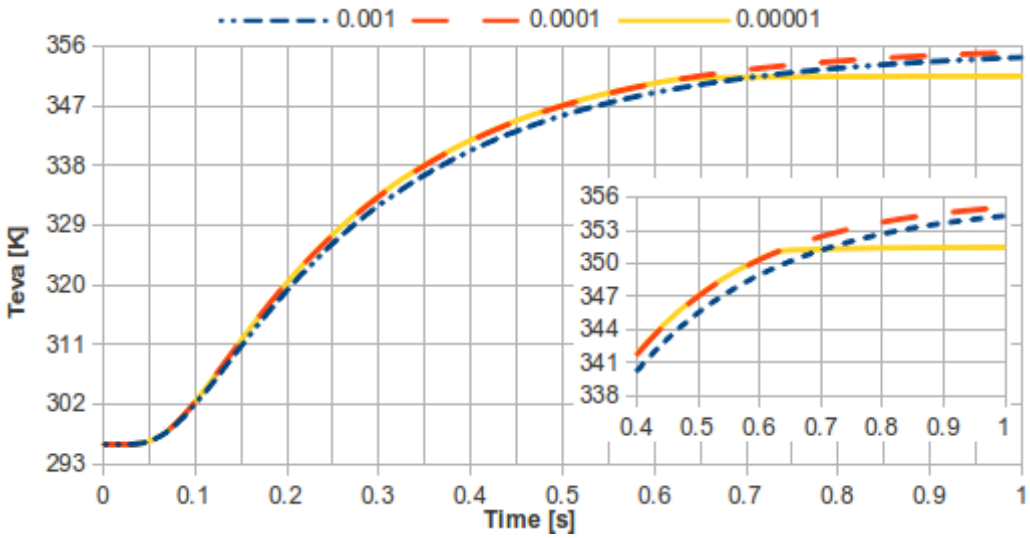

Figure 5.14 Evaporator temperature with conditioning solution for different time steps

Better results are indeed provided by under-relaxation technique. **Under-relaxation method** operates by limiting the amount which a variable changes from one iteration to the next by modifying the field of temperature directly. An under-relaxation factor ω $(0 \leq \omega \leq 1)$ specifies the amount of under-relaxation, ranging from none at all for $\omega = 1$ and increasing in strength as $\omega \to 0$, while the limiting case where $\omega = 0$ represents a solution which does not change at all with successive iterations. A correct choice for ω results from a trade-off between numerical stability (small values of ω) and computational time (large values of ω); values of ω as high as 0.9 can ensure stability in some cases and anything much below, such as 0.2, is prohibitively restrictive in slowing the iterative process.
Under-relaxation technique is applied to the heat pipe evaporator temperature T_{eva}, that is evaluated for each iteration as follows:

$$T_{\text{eva}}^{\text{n+1}} = (1-\omega)T_{\text{eva}}^{\text{n}} + \omega\tilde{T}_{\text{eva}}^{\text{n+1}} \qquad (5.14)$$

The effect of relaxation factor on numerical propagation is shown in Figure 5.15. Using low values of relaxation factor (e.g. 0.1, 0.3) propagation is too slow or even wrong; while too high values (e.g. 0.9) are insufficient to ensure numerical stability. Then a relaxation factor of 0.5 for the temperature field has been selected; for each step of the fixed-point iteration the temperature $T_{\text{eva}}^{\text{n+1}}$ is the average value between two successive iterations.

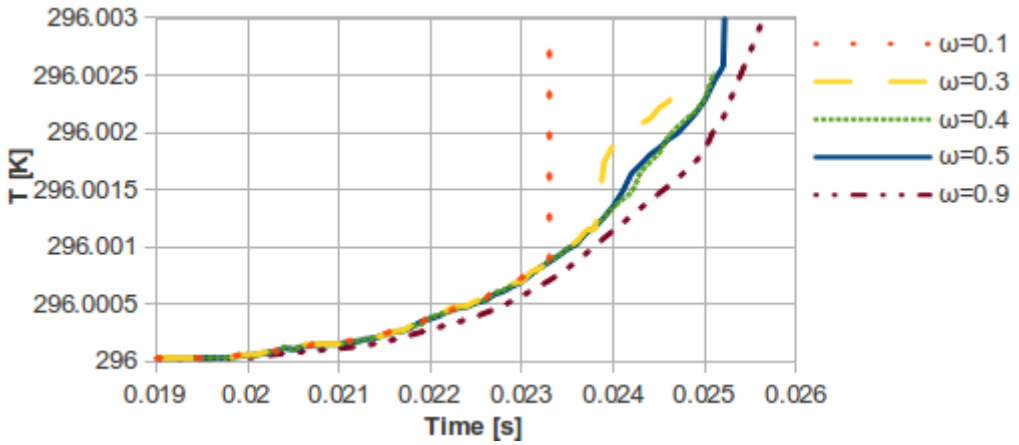

Figure 5.15 Effects of relaxation-factor on numerical propagation

The new algorithm is able to damp out the approximation errors and it is numerically stable.

The flowchart of Figure 5.9 is then updated as shown in Figure 5.16.

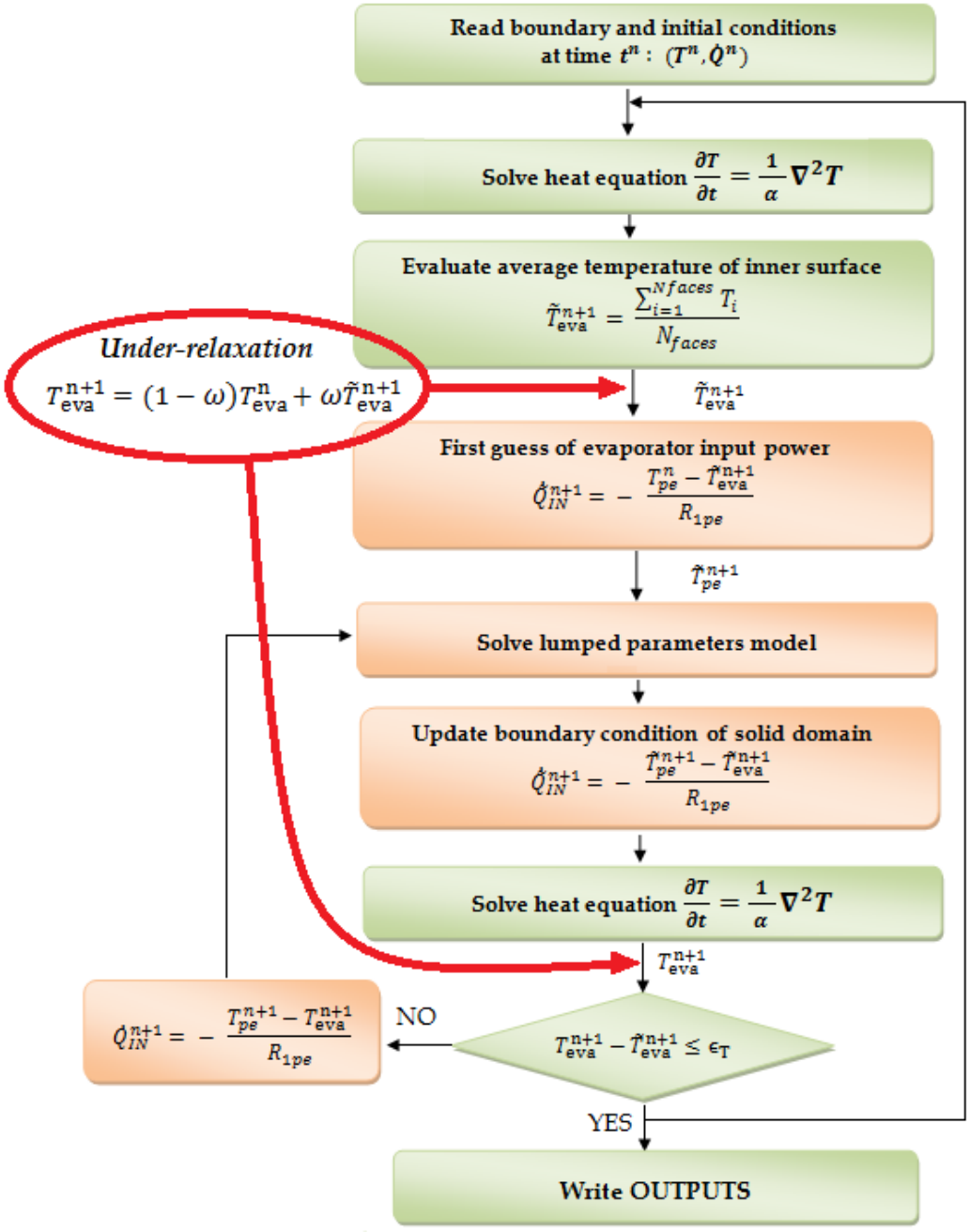

Figure 5.16 Flowchart of hybrid solver with under-relaxation technique
red blocks: lumped parameter model
green blocks: finite volumes model

5.5 Hybrid analysis

The hybrid analyses proposed in the present paragraph are test cases used to determine whether the hybrid solver is working correctly or not. With this purpose results are compared with an equivalent analysis performed by COMSOL Multiphysics, a finite element analysis software for engineering applications. COMSOL simulations represent the typical approach used to simulate the presence of heat pipe in a finite element analysis. Heat pipe is modeled as a solid cylinder (see Figure 5.17) with the following equivalent properties:

- the specific heat of heat pipe's material,
- a mean thermal conductivity derived from experimental data (typically 4000-6000 W/m K),
- an equivalent density defined as follows

$$\rho_{eq} = \frac{m_{HP}}{V_{HP}} \tag{5.15}$$

where m_{HP} and V_{HP} are respectively the mass and the volume of heat pipe.

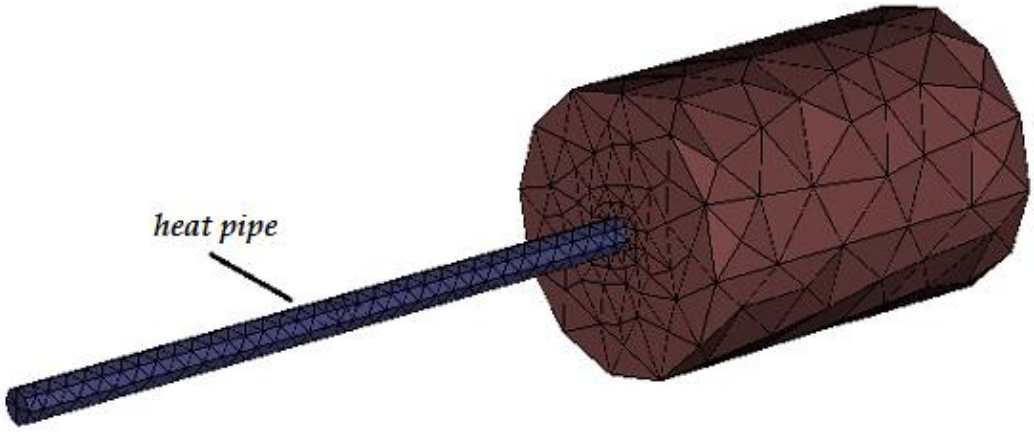

Figure 5.17 Finite element model of heat pipe embedded in solid domain

The analysis performed by hybrid solver in OpenFOAM environment refer to a solid domain representing a cylinder shaped tube (see Figure 5.18) whose sizes are summarized in Table 5.2.

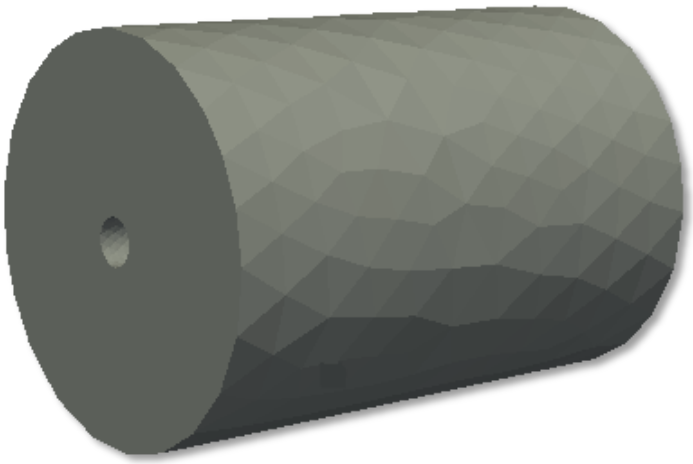

Figure 5.18 Solid domain of hybrid analysis

Table 5.2 Geometric properties of solid domain

Cylinder's geometry	
Outer diameter [mm]	50
Thickness [mm]	2.2
Length [mm]	70

The water-copper heat pipe has the geometric features listed in Table 5.3.

Table 5.3 Heat pipe's properties for hybrid analysis

Heat pipe's geometry			
d_{ep} **[mm]**	6	L_{eva} **[mm]**	70
d_{ip} **[mm]**	5	L_{a} **[mm]**	60
d_{iw} **[mm]**	4	L_{cond} **[mm]**	50
Wick's properties			
ε	0.7	r_g **[μm]**	50

The results of the analysis refer to simulations with different boundary conditions at heat pipe's condenser section, specifically

1) Imposed temperature,
2) Convective condition.

The top and the base of the cylinder are assumed to be adiabatic surfaces. At start time heat pipe and solid domain have the same temperature T_0. Mass flow rates are assumed to be equal to zero.

5.5.1 Simulation 1 - Imposed temperature

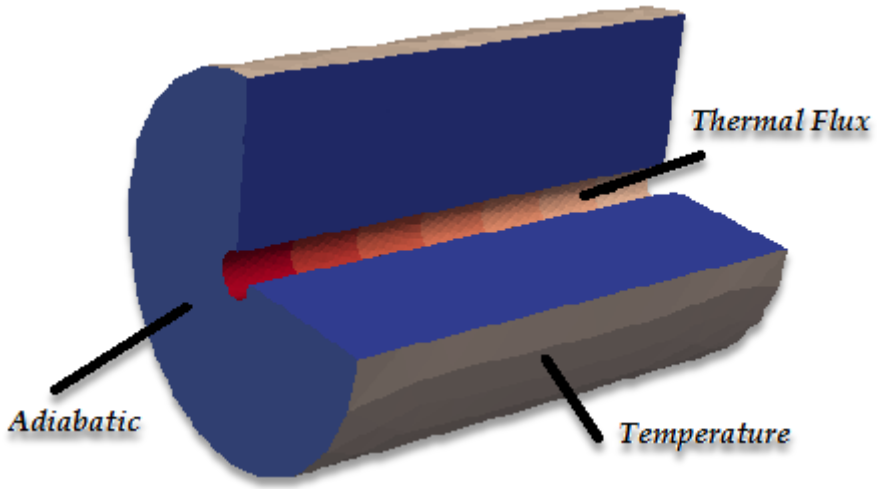

Figure 5.19 Simulation 1 - Boundary conditions

The simulation inputs are specified in Table 5.4 . The boundary conditions are also schematically illustrated in Figure 5.19.

Table 5.4 Simulation 1: inputs

Initial and boundary conditions	
Initial temperature T_0 [K]	293
Outer wall temperature [K]	363
Condenser temperature T_{cond} [K]	293
Cylinder's thermal property	
Diffusivity α [m²/s]	0.0005
Simulation control parameters	
End time [s]	2.5
Time step	0.0001

The evaporator temperature of heat pipe is illustrated in Figure 5.20. Heat pipe achieves a steady-state condition (355.4 K) after 1 second since the thermal diffusivity is relatively high if compared with common metals properties (e.g., copper's thermal diffusivity is about 1.1×10^{-4} m^2/s).

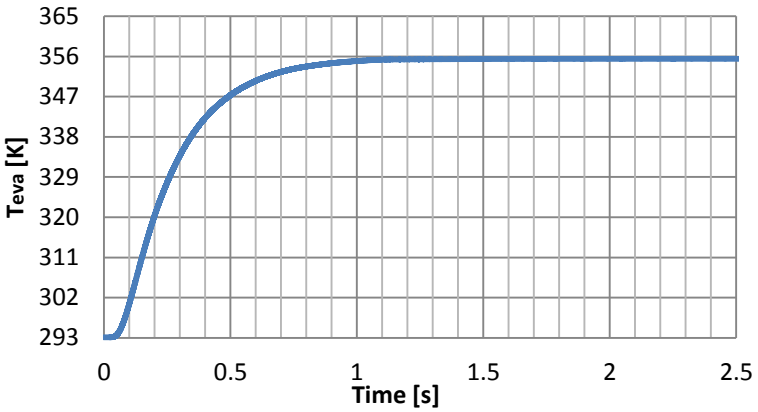

Figure 5.20 Simulation 1 - Evaporator temperature

Figure 5.21 shows a detail of evaporator temperature's graph in order to illustrate the temperature trend at the beginning of transient phase.

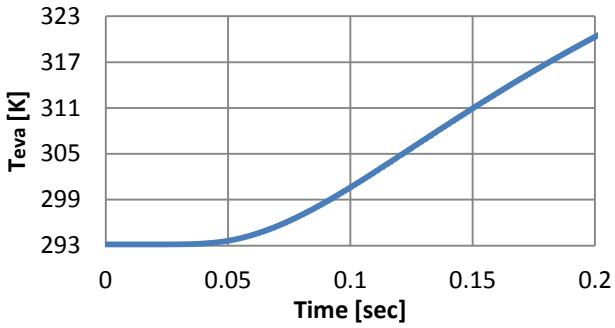

Figure 5.21 Simulation 1 - Evaporator temperature at the beginning of transient phase

The hybrid analysis solution is compared with the results of the finite element analysis performed by COMSOL Multiphysic, where the heat pipe is represented by a finite element model of a three-dimensional cylinder with the equivalent properties listed in Table 5.5. The two analysis are equivalent in terms of geometric features, initial and boundary conditions, as shown in Figure 5.22.

Table 5.5 COMSOL simulation - Heat pipe's equivalent properties

Physical properties	
ρ **[kg/m³]**	3395
k **[W/m K]**	4000
c **[J/kg K]**	380

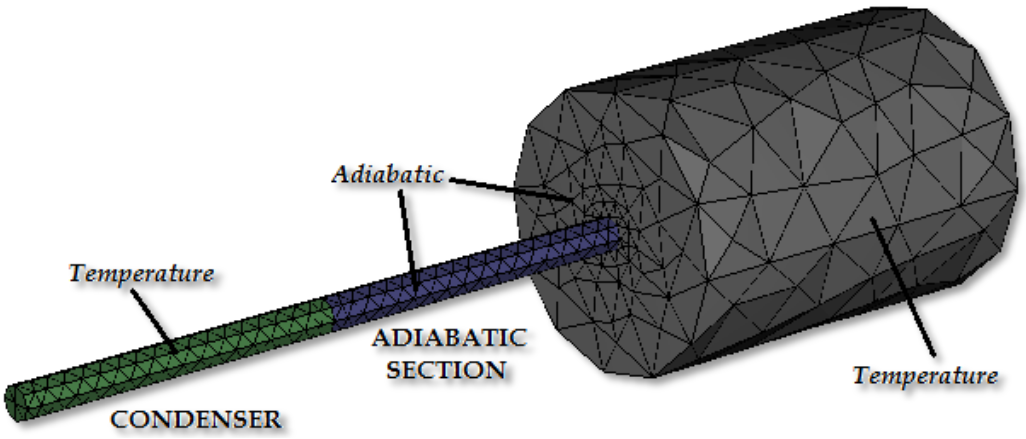

Figure 5.22 COMSOL simulation 1 - Boundary conditions

The results of the two analyses are compared in Figure 5.23 by means of evaporator wall temperature. The temperature curves match in transient phase but they achieve different steady-state conditions. In COMSOL simulation the steady-state temperature is the temperature imposed on the outer surface of external domain since the finite element model does not account for the equivalent convective resistance of heat pipe. At heat pipe/solid domain interface the continuity of conductive power is imposed, while the heat pipe is better represented by an equivalent convective power.

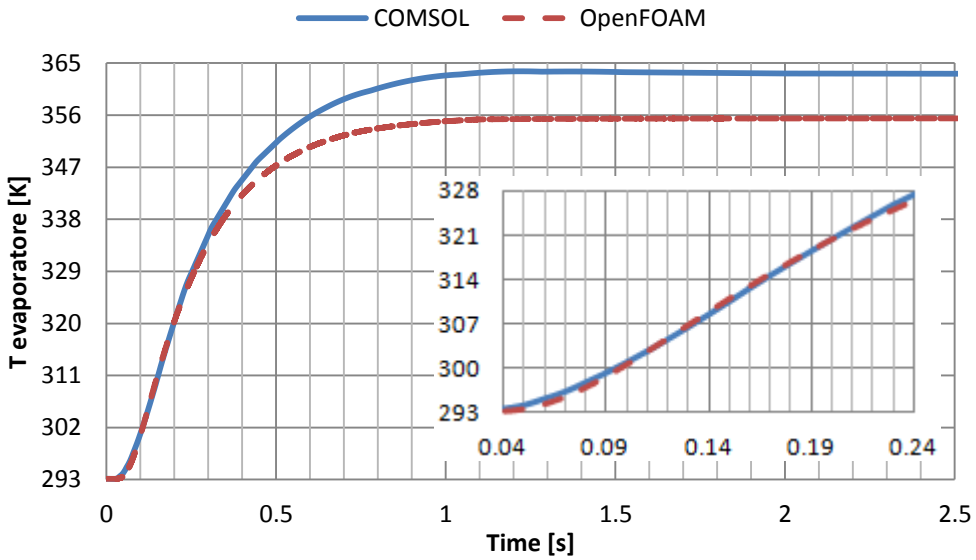

Figure 5.23 Simulation 1 - Comparison of solutions obtained by COMSOL and OpenFOAM

5.5.2 Simulation 2 - Convective condition

The analysis with a convective condition at condenser section of heat pipe represents one of the most common operational conditions of heat pipes.
The boundary conditions of solid domain are the same as the simulation proposed in paragraph 5.5.1 and they are schematically illustrated in Figure 5.19, while heat pipe's boundary condition is converted in a cooling convective condition at condenser section.
The simulation inputs are specified in Table 5.6.

Table 5.6 Simulation 2 – Inputs of hybrid solver

Initial and boundary conditions	
Initial temperature T_0 [K]	293
Outer wall temperature [K]	363
Cooling fluid properties	
T_f [K]	283
h_f [W/m²K]	400
Cylinder's thermal property	
Diffusivity α [m²/s]	0.00009
Simulation control parameters	
End time [s]	6
Time step	0.0001

The temperature field distribution in solid domain is illustrated in Figure 5.25 and Figure 5.26.

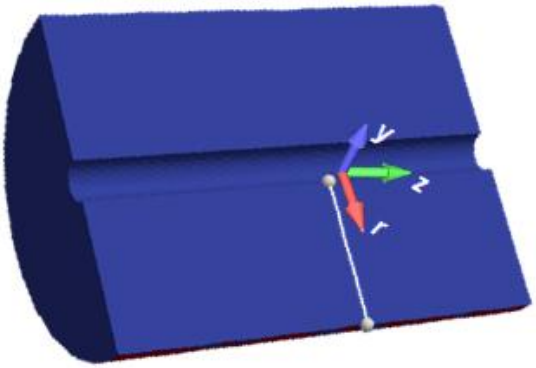

Figure 5.24 Coordinate reference system of solid domain

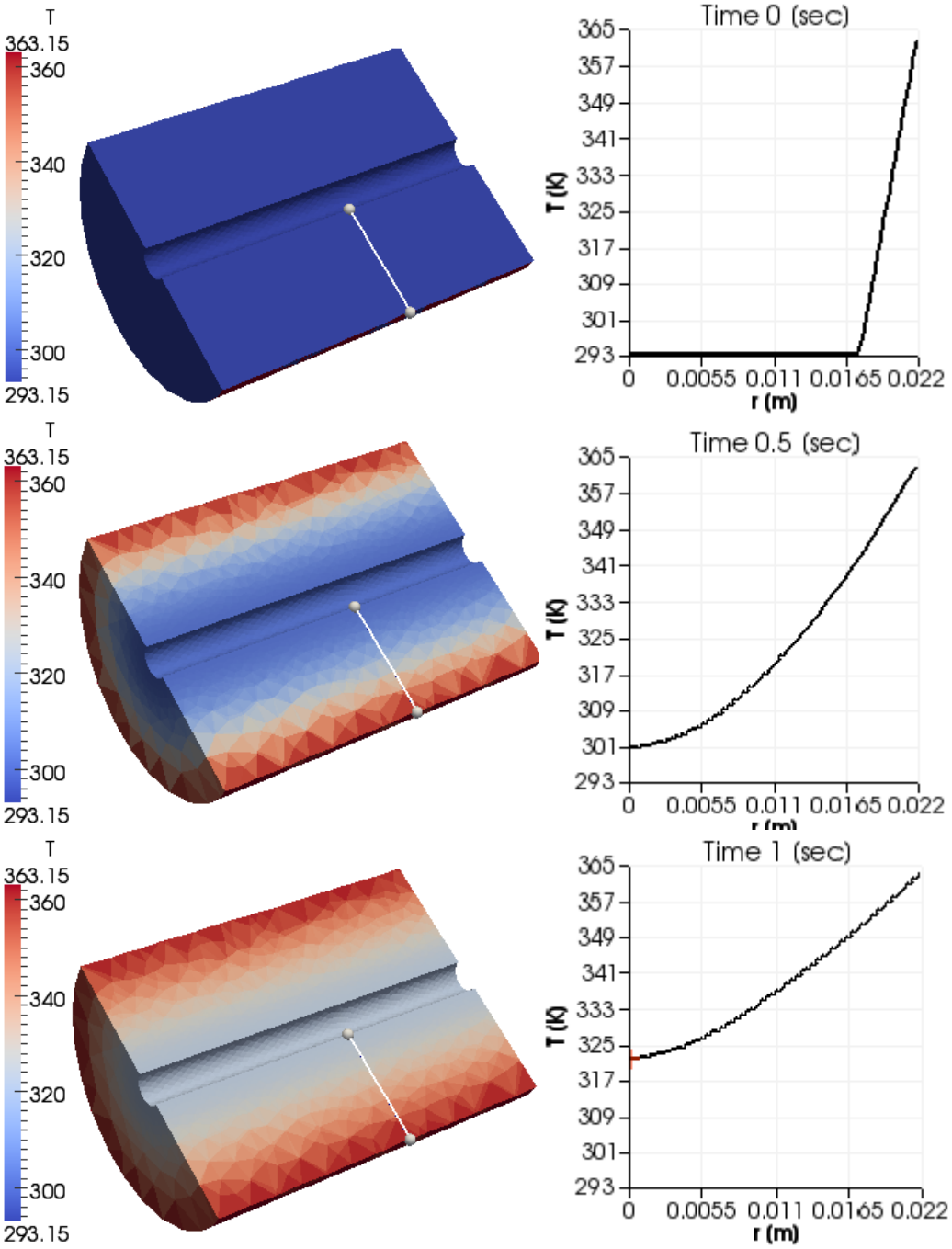

Figure 5.25 Simulation 2 - Temperature field in solid domain at time 0s, 0.5s, 1s

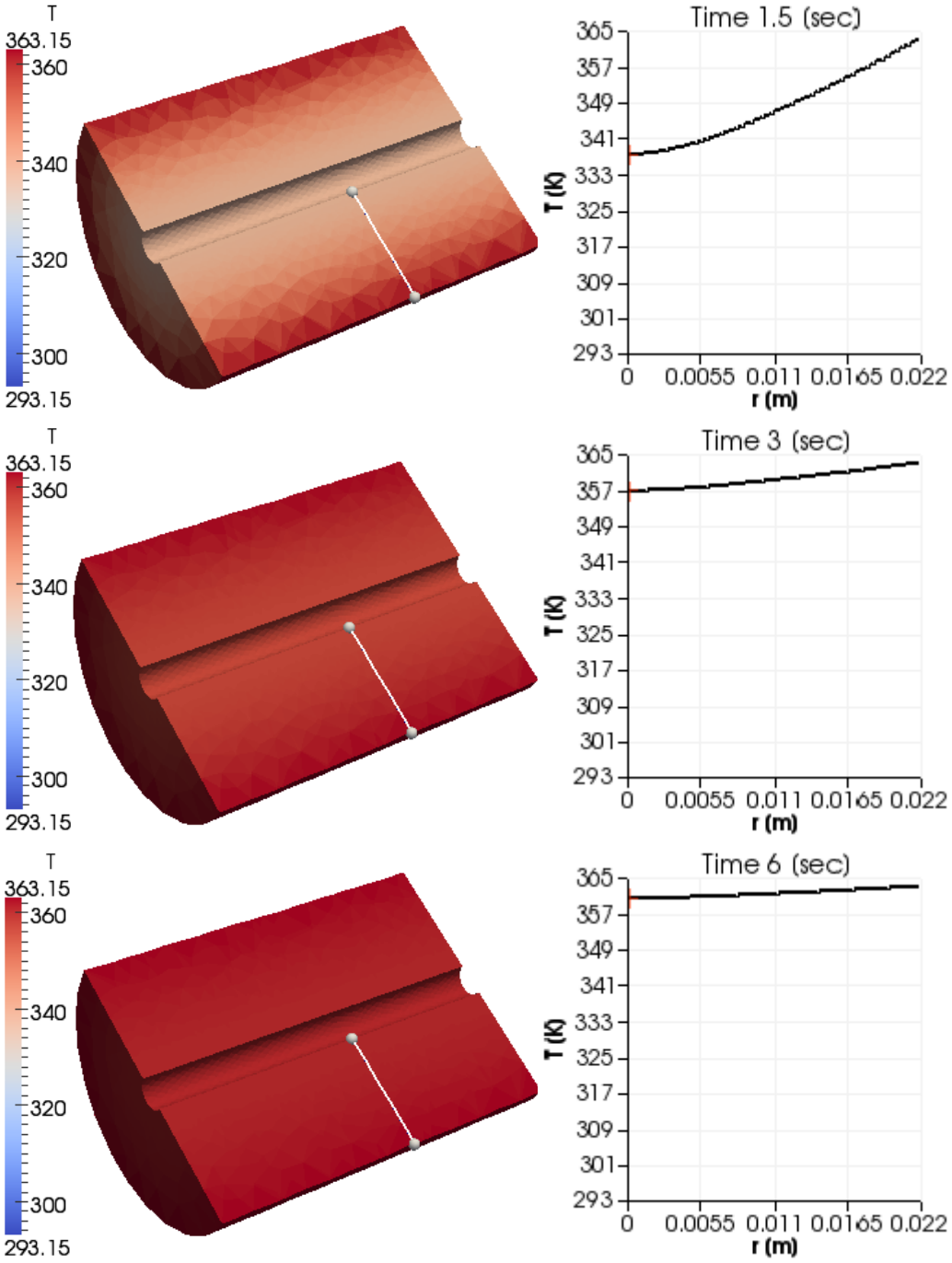

Figure 5.26 Simulation 2 - Temperature field in solid domain at time 1.5s , 3s, 6s

The graphs of Figure 5.25 and Figure 5.26 represent the temperature trend in function of radius in according to the coordinate reference system of Figure 5.24.

Figure 5.27 illustrates the heat pipe temperatures of evaporator and condenser outer walls and the vapor temperature. Heat pipe achieves steady-state condition within 4 seconds, a longer time compared to preceding simulation since solid domain has a lower thermal diffusivity ($9x10^{-5}$ vs. $5x10^{-4}$). The outer surface temperature of condenser section decreases tending asymptotically to cooling fluid temperature.

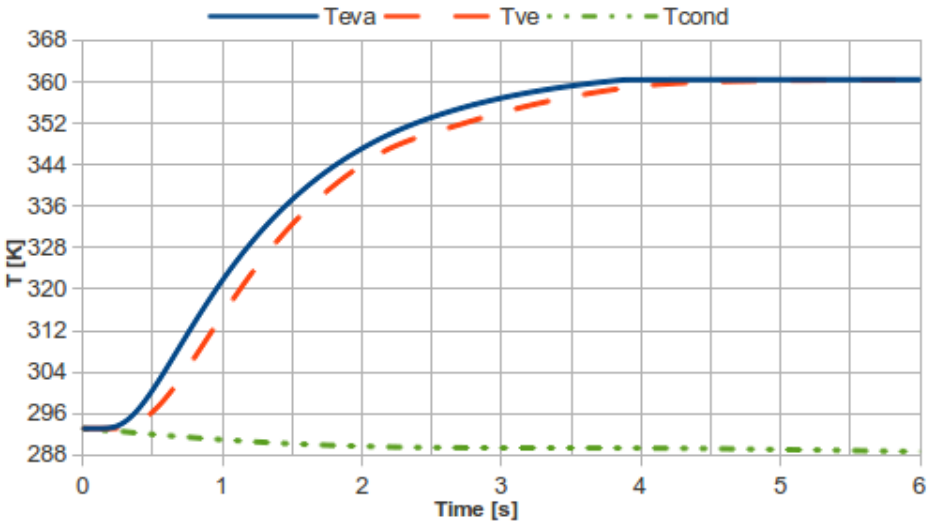

Figure 5.27 Temperatures of evaporator and condenser wall (T_{eva}, T_{cond}) and vapor temperature (T_{ve})

The hybrid analysis solution is compared with the results of the finite element analysis performed by COMSOL Multiphysic. Equivalent properties of heat pipe are listed in Table 5.5. Boundary condition are schematically illustrated in Figure 5.28.

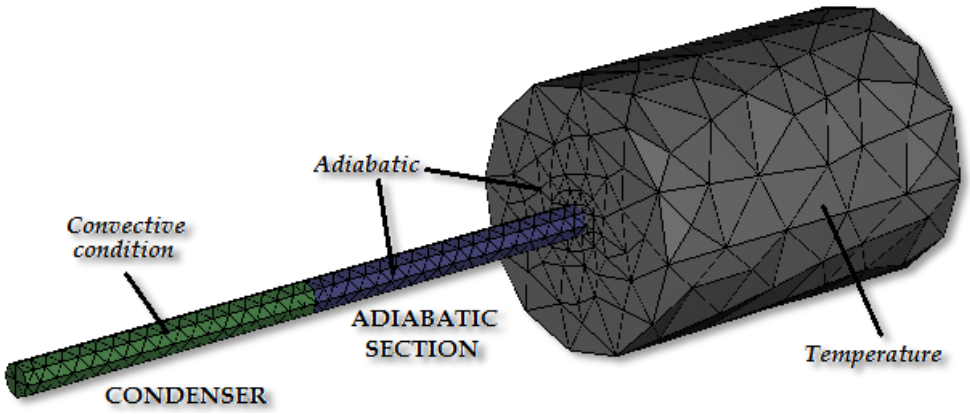

Figure 5.28 COMSOL simulation 2 - Boundary conditions

Figure 5.29 compares the evaporator temperature of heat pipe obtained by COMSOL and OpenFOAM simulations. Temperature trend is obviously similar but the temperature jump in each time step is not negligible. However the rough solution obtained by COMSOL could be useful for a preliminary design.

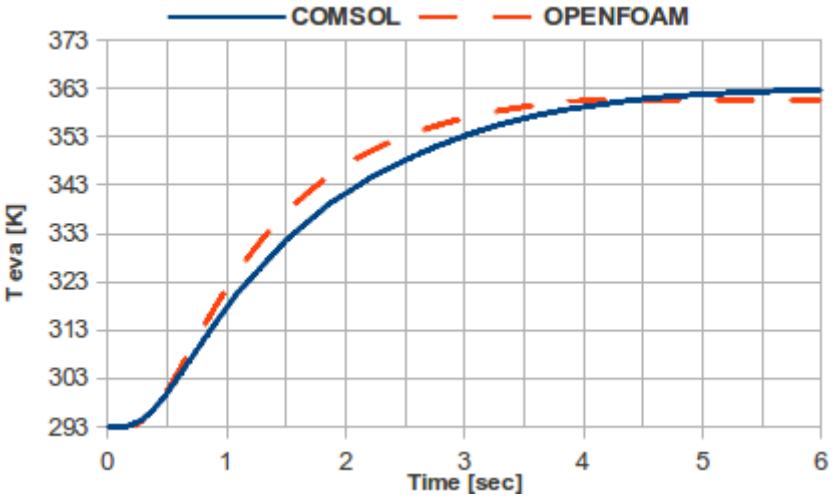

Figure 5.29 Simulation 2 - Comparison of solutions obtained by COMSOL and OpenFOAM

6 Conclusions

The numerical coupling of a heat pipe lumped parameter model and a finite element model of an external solid domain is addressed. The analyses performed by the hybrid solver are similar to the finite element analyses where heat pipe is modeled as a solid cylinder of highly conductive material. However the results of finite element model are highly dependent from equivalent heat pipe thermal conductivity obtained by experimental data and then from the specific heat pipe features.

Results supplied by lumped parameter model will be useful to evaluate heat pipes performances and to understand heat pipe behavior in different operative conditions. Furthermore the coupled analysis allows to optimize heat pipe design for a specific application providing the best fit of the heat pipe geometrical parameters depending on the external solid domain boundary conditions.

The hybrid analysis results will be further validated by experimental data as soon as the experimental apparatus will be set up. Then experimental data will be useful to definitively validate and improve numerical model.

The simulations presented in this work are test cases. The importance of a coupled analysis is more evident for complex geometries of external domain when transient boundary conditions are applied, (i.e., simulation of heat pipe operation during mould's heat-up and cool-down process).

In further developments the condenser section of the lumped parameter model will be also coupled to external solid domain, since the condenser section is not always in direct contact with cooling fluid but it is surrounded by a cooling fin structure in order to increase the heat transfer area resulting in enhanced heat exchange. On the other hand the lumped parameter model will be coupled to an optimization program (i.e., GenOpt, OpenOpt) in order to provide a real optimization of heat pipe performances.

Nomenclature

Variable	Description	Units
A	Area	[m²]
$\underline{\boldsymbol{A}}$	Matrix of coefficient of linear system	-
$\boldsymbol{B}$	Input vector of linear system	-
C	Thermal capacitance	[W/K]
c	Specific heat	[J/kg K]
c_p	Specific heat at constant pressure	[J/mol K]
c_v	Specific heat at constant volume	[J/mol K]
D	Diameter	[m]
F	Frictional coefficient	[-]
f	Correction coefficient for pressure	[-]
h	Convective heat transfer coefficient	[W/m² K]
h_{lv}	Latent heat of vaporization/condensation	[J/kg]
K	Permeability	[m²]
k	Thermal conductivity	[W/m K]
L	Length	[m]
$\bar{L}$	Fluidic inductance	[1/m]
$\underline{\boldsymbol{L}}$	Lower matrix of LU decomposition	-
M	Liquid mass	[kg]
Me	Liquid mass in the evaporator wick	[kg]
Me_0	Maximum liquid mass in the evaporator wick	[kg]
$\dot{m}$	Mass flow rate	[kg/s]
Nu	Nusselt number	[-]
$\underline{\boldsymbol{P}}$	Permutation matrix of LU decomposition	-
p	Pressure	[Pa]
Pr	Prandtl number	[-]
$\dot{Q}$	Heat power	[W]
$\check{\dot{Q}}$	Approximated heat power	[W]
R	Thermal resistance	[K/W]
$\bar{R}$	Fluidic resistance	[Pa s/kg]
R^*	Specific gas constant	[J/kg K]
r	Radius	[m]
Re	Reynolds number	[-]
t	Time	[s]

Variable	Description	Units
T	Temperature	[K]
$\tilde{T}$	Approximated temperature	[K]
$\mathbf{U}$	Darcy flux	[m/s]
$\mathbf{u}$	Velocity	[m/s]
$\underline{\boldsymbol{U}}$	Upper matrix of LU decomposition	-
V	Volume	[m^3]
$\boldsymbol{x}$	Vectors of unknown of LU decomposition	-
$\boldsymbol{y}$	Vector of unknowns of linear system	-
Δt	Time step	[s]
γ	Heat capacity ratio	[-]
ε	Wick porosity	[-]
μ	Dynamic viscosity	[Pa s]
ρ	Density	[kg/m^3]
σ	Surface tension	[Pa m]
χ	Level of dryness	[-]
ω	Under-relaxation factor	[-]

Subscripts

0	Initial condition
1	Section 1
2	Section 2
a	Adiabatic
c	Capillary
cond	Condenser
conv	Convective
eff	Effective
eq	Equivalent
eva	Evaporator
ext	External
ew	External wick
f	Cooling fluid
g	Grains
HP	Heat Pipe
IN	INPUT
int	Internal
iw	Internal wick
l	Liquid
lc	Wick condenser liquid
le	Wick evaporator liquid
lv	Liquid/vapor
pa	Adiabatic pipe
pc	Condenser pipe
pe	Evaporator pipe
v	Vapor
va	Adiabatic vapor
vc	Condenser vapor
ve	Evaporator vapor
w	Solid wick/Wick liquid
wa	Adiabatic wick
wc	Condenser wick
we	Evaporator wick

Acronyms

CAD	Computer-Aided Design
CFD	Computational Fluid Dynamics
ENCOM	ENhanced Condensers and related phenOmena in two-phase systeMs
FVM	Finite Volume Method
GSL	GNU Scientific Library
HP	Heat Pipe
ISS	International Space Station
NCG	Non Condensable Gases
NIST	National Institute of Standards and Technology
ODE	Ordinary Differential equations

Bibliography

[1] Y. Cao, A. Faghri, Transient two-dimensional compressible analysis for high temperature heat pipe with pulsed heat input, *Numerical Heat Transfer*, **114**, (1990), 1028-1035.

[2] Z.J. Zuo, A. Faghri, A network thermodynamic analysis of the heat pipe, *International Journal of Heat and Mass Transfer*, **41**, (1998), 1473-1484.

[3] N. Zhu, K. Vafai, Analysis of cylindrical heat pipes incorporating the effects of liquid-vapor coupling and non-Darcian transport-a closed form solution, *International Journal of Heat and Mass Transfer*, **42**, (1999), 3405-2418.

[4] V.H. Ransome, H. Chow, ATHENA heat pipe transient model, *Trans. 4th Symposium on Space Nuclear Power System*, CONF-870102, Albuquerque, (1987), 389-392.

[5] J.M. Tournier, M.S. El-Genk, A heat pipe transient analysis model, *International Journal of Heat and Mass Transfer*, **37**, (1994), 753-762.

[6] C. Ferrandi, F. Iorizzo, M. Mameli, Stefano Zinna, M. Marengo, LUMPED PARAMETER MODEL OF SINTERED HEAT PIPE, NUMERICAL ANALYSIS AND VALIDATION. Submitted to *Applied Thermal Engineering*, (2012).

[7] A. Quarteroni, S. Ragni, A. Veneziani, Coupling between lumped and distributed models for blood flow problems, *Compunting and Visualization in Science*, **4**, (2001), 111-124

[8] J.F. Wenk, L. Ge, Z. Zhang, M. Soleimani, D.D. Potter, A.W. Wallace, E. Tseng, M.B. Ratcliffe, J.M. Guccione, A coupled biventricular finite element and lumped-parameter circulatory system model of heart

failure, *Computer Methods Biomechanics and Biomedical Engineering*, (2012)

[9] H.J. Kim, I.E. Vignon-Clementel, C.A. Figueroa, J.F. LaDisa, K.E. Jansen, J.A. Feainstein, C.A. Taylor, On coupling a lumped parameter heart model and a three-dimensional finite element aorta model, *Annals of Biomedical Engineering*, **37**, (2009), 2153-2169

[10] C. Ferrandi, M. Marengo, S. Zinna, Influence Of Tube Size On Thermal Behavior Of Sintered Heat Pipe, Proc. 2nd European Conference on Microfluidics - Microfluidics 2010 - Toulouse, December 8-10, 2010, Copyright SHF, ISSN 2108-4718, ISBN 978-2-906831-85-8

[11] G. P. Peterson, An introduction to Heat Pipes, Wiley Series in Thermal Management of Microelectronic & Electronic Systems Allan D. Kraus and Avram Bar-Cohen, Series Editors, 1994.

[12] S. W. Chi, Heat Pipe Theory and Practice, a Sourcebook, *Hemisphere Publishing Corporation*, 1976.

[13] M.S. El-Genk, L. Huang, An experimental investigation of the transient response of a water heat pipe, *International Journal of Heat and Mass Transfer*, **36, (15)**, (1993), 3823-3830.

[14] K.C. Leong, C.Y. Liu, Characterization of a Copper Wicks Used in Heat Pipe, *Journal of porous material*, **4**, (1997), 303-308.

[15] Cotter, T.P. Principles and prospects for micro heat pipes, Proceedings of 5th International Heat Pipe Conference, 1, Tsukuba. (1984), 328–335.

[16] Lemmon E.W., H. M. (2007). NIST Standard Reference database 23: Reference Fluid Thermodynamic and Transport Properties. *National Institute of Standards and Technology*

[17] J. Ochterback, *HEAT TRANSFER HANDBOOK* (Vol. 16). Hoboken, New Jersey: A. Bejan, A.D. Kraus, John Wiley & Sons, Inc. (2003)

[18] OpenFOAM, F. (n.d.). *OpenFoam*. Retrieved Febbraio 29, 2012, from http://www.openfoam.org/archive/2.0.0/docs/user/userch1.php#x3-20001